Cosmic Rays and Diffuse Galactic Gamma-Ray Emission

Igor Moskalenko & *Andrew Strong*

NRC & NASA GSFC *MPE, Garching*

- Introduction
- Modelling approach
- Nuclei in CR & propagation parameters
- Diffuse gamma rays & tests of the nucleon spectrum
- An application (WIMP search)

Main references:

ApJ 1998, 493, 694 (positrons & electrons)
A&A 1998, 338, L75 (antiprotons & test of the nucleon spectrum)
ApJ 1998, 509, 212 (nuclei & numerical scheme)
Phys.Rev.D 1999, 60, 063003 (positrons from the dark matter)
ApJ 2000, 528, 357 (anisotropic inverse Compton scattering)
ApJ 2000, 537, in press (diffuse continuum gamma rays)

Overviews:

ASP Conf. Ser. 1999, 171, 162
Proc. 5th Compton Symp. 2000, AIP, in press

Our results and software are available on WWW:

http://www.gamma.mpe-garching.mpg.de/~aws/aws.html

Introduction
Interactions in the ISM
Links between branches of CR physics

Modelling approach
Galprop model
Isotope table
Equation
Interstellar radiation field & anisotropic IC scattering
An effect of anisotropic IC scattering
3D distribution
GALPROP parameters & constraints

Nuclei in CR & propagation parameters
B/C diffusion/convection no break
B/C diffusion/convection with break
B/C with reacceleration
10Be reacceleration
10Be convection
Other recent estimates
B/C and subFe/Fe
Some other ratios
Isotopic abundances
Gradients
SNR distribution (Case & Bhattacharya 1996)

Diffuse gamma rays & tests of the nucleon spectrum
Conventional model
Unidentified sources
Hard Nucleons model
Electrons & synchrotron index
Hard Electrons model
Hard Electrons & Modified Nucleons model
Synchrotron profiles
Longitude and latitude profiles
High latitudes
Electron spec. + Baring

An application (WIMP search)
Green's functions
WIMP positrons

Some other pictures
Interstellar radiation field
Reacceleration formalism
Interstellar gas distribution
SNR distribution (Case & Bhattacharya 1998)
pbar/p ratio
Enlarged 70-100 MeV profile
Parameters & objectives of models

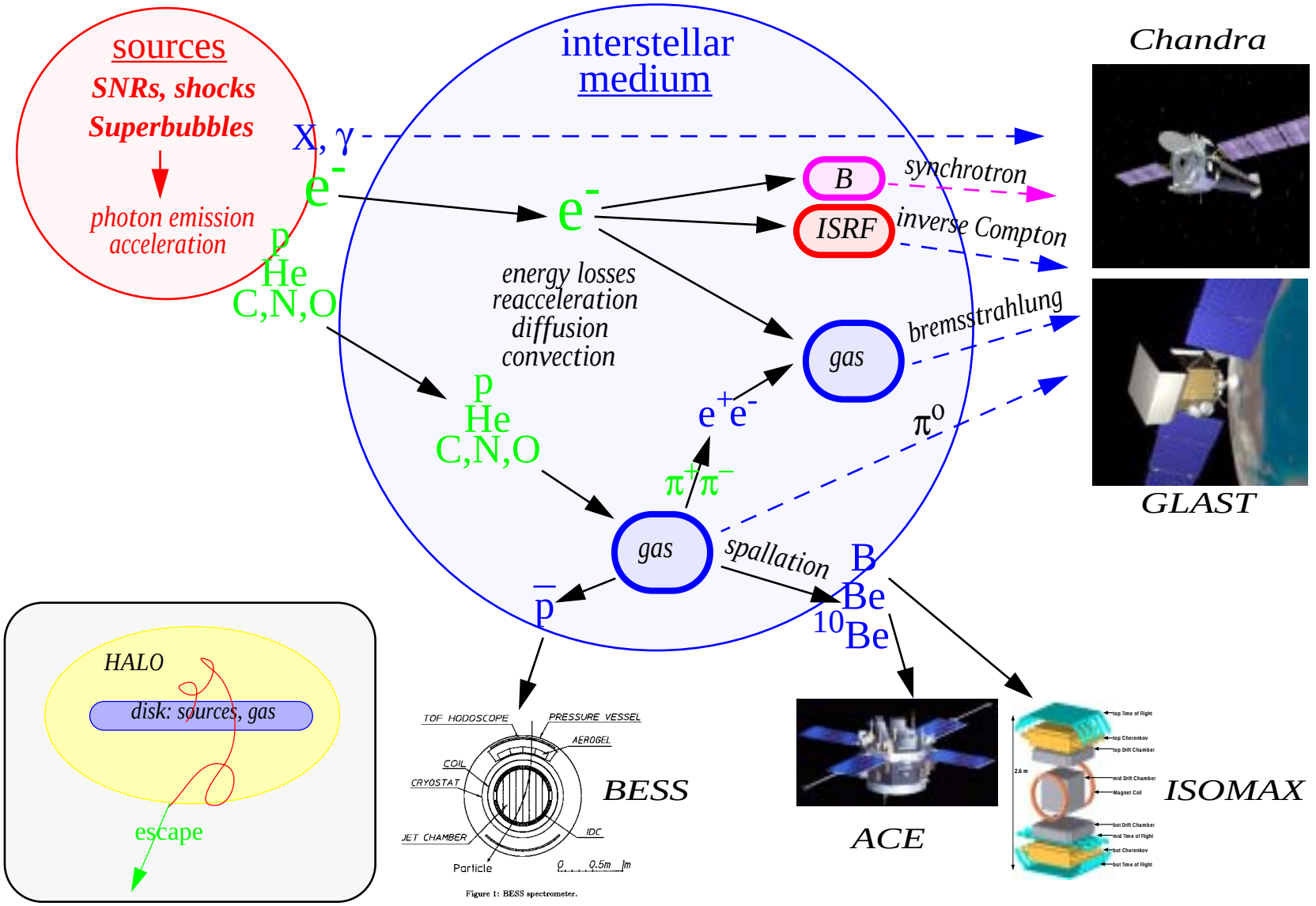
sources
SNRs, shocks
Superbubbles
photon emission
acceleration
interstellar
medium
X, γ
e-
p
He
C,N,O
e-
B
synchrotron
ISRF
inverse Compton
energy losses
reacceleration
diffusion
convection
gas
bremsstrahlung
p
He
C,N,O
e+e-
π0
π+π−
gas
spallation
B
Be
10Be
p̄
Chandra
GLAST
HALO
disk: sources, gas
escape
TOF HODOSCOPE
PRESSURE VESSEL
AEROGEL
COIL
CRYOSTAT
JET CHAMBER
IDC
Particle
0 0.5m 1m
BESS
ACE
ISOMAX
Figure 1: BESS spectrometer.

Some links between branches of cosmic ray physics

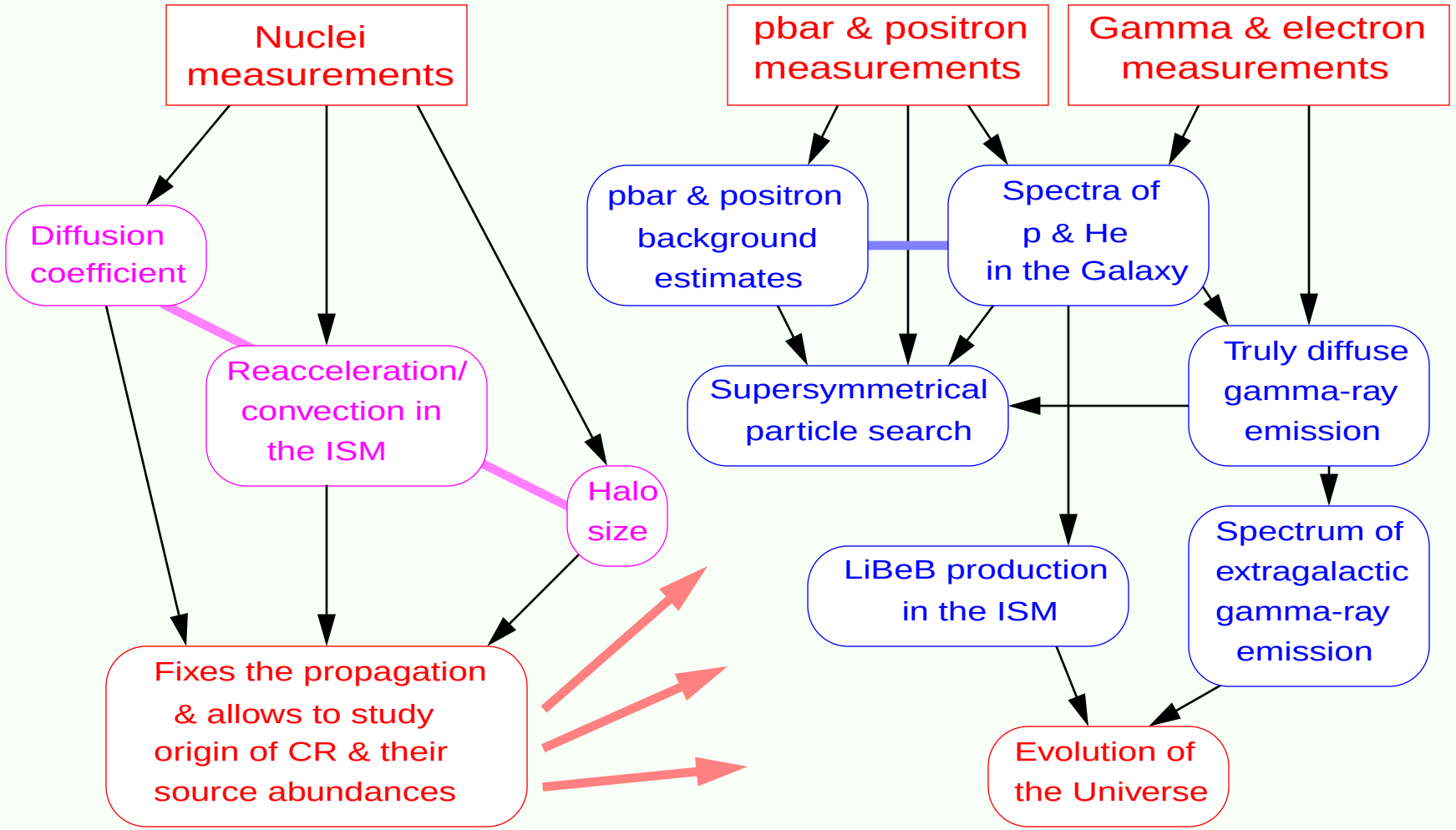

‘galprop’ model

Galactic CR propagation numerically in 3D

$f(R, z, p)$

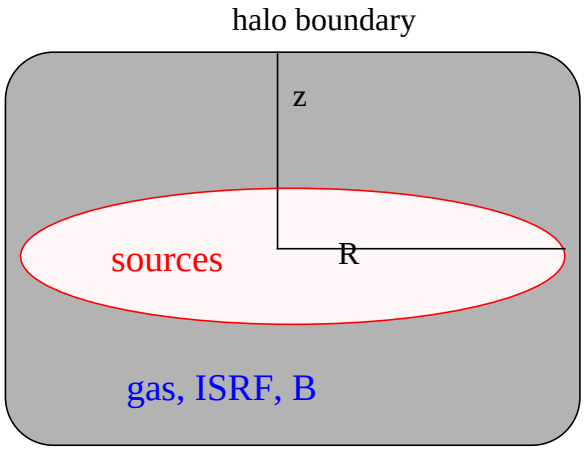

realistic gas, radiation fields
source distribution can be chosen

diffusion, convection, reacceleration
energy losses

propagation of primaries,
secondaries, tertiaries etc.

nuclear reaction network

γ-rays, synchrotron computed consistently

current version includes:

$\overline{p}, e^+, e^-, \gamma$–, *synchrotron emission*
+ All 87 stable & long-lived isotopes H-> Ni !

program available on WWW

Table of Isotopes (1999)

Z=0-28 Part 1 of 2

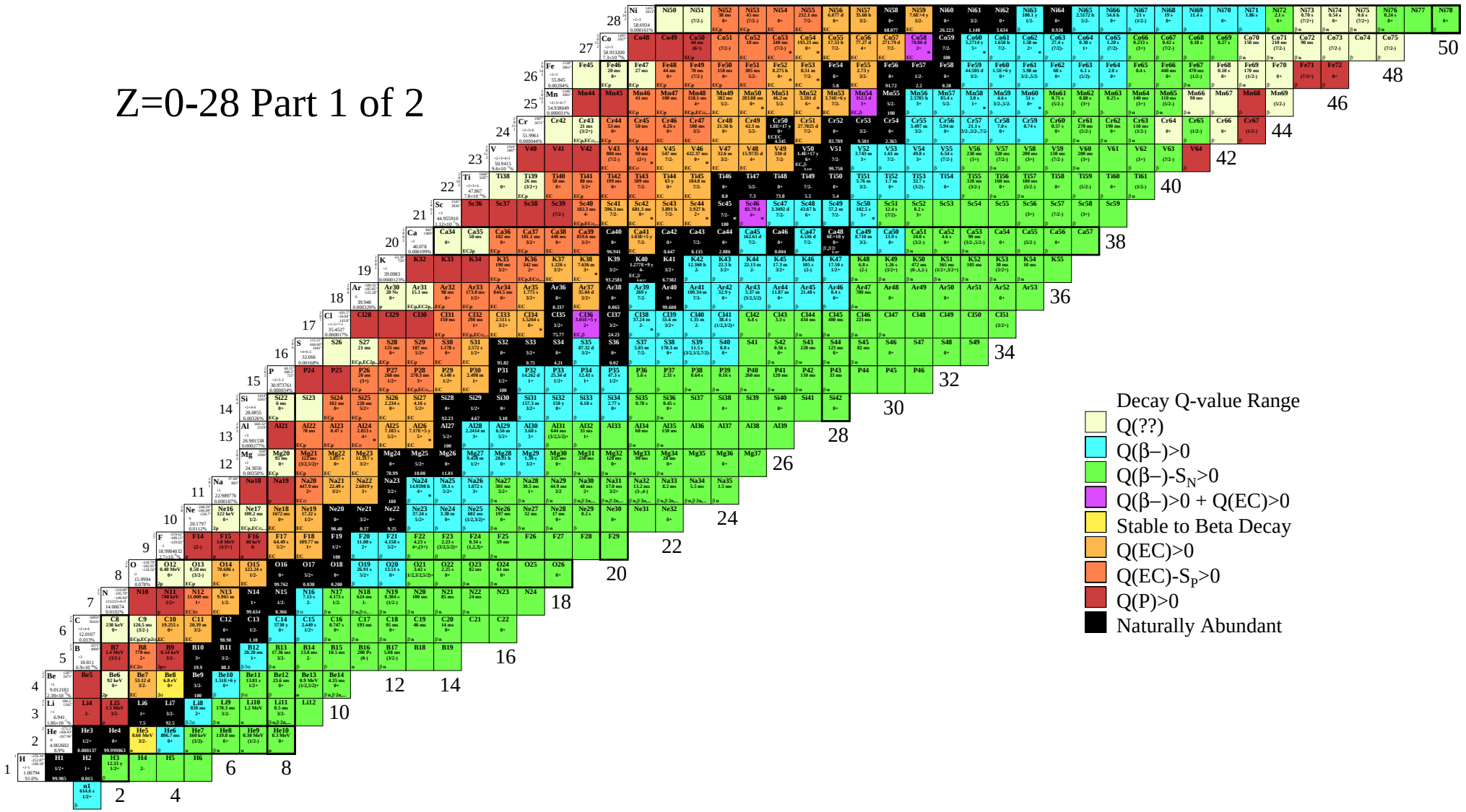

Cosmic Ray Propagation Model

$$\frac{\partial}{\partial t}\psi(\vec{r},p,t) =$$

$$q(\vec{r},p) \quad \textit{sources}$$

$$+\vec{\nabla}.[D_{xx}\vec{\nabla}\psi - \vec{V}\psi]$$

diffusion *convection*

$$+\frac{\partial}{\partial p}[p^2 D_{pp}\frac{\partial}{\partial p}\frac{\psi(p)}{p^2}]$$

diffusive reacceleration

$$-\frac{\partial}{\partial p}[(\frac{dp}{dt} - \frac{1}{3}p\vec{\nabla}.V)\psi]$$

energy loss *convection*

$$-\frac{\psi}{\tau_i} - \frac{\psi}{\tau_r}$$

fragmentation *radioactive decay*

Interstellar Radiation Field

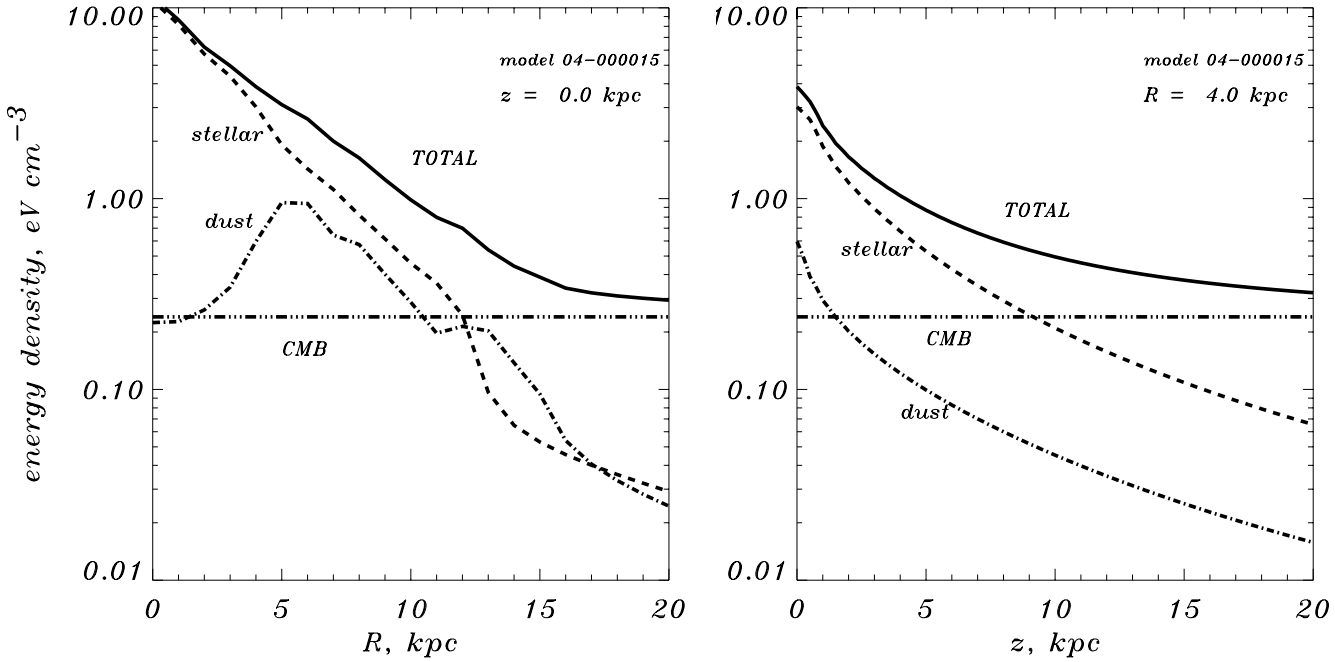

Anisotropic Inverse Compton Scattering

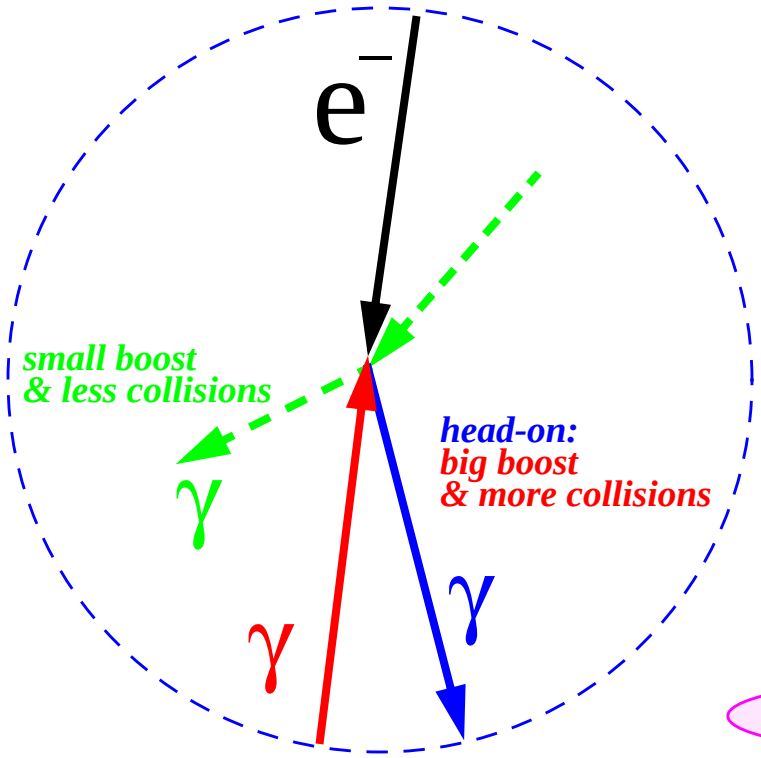

electrons in halo see anisotropic radiation:
head-on collisions are seen by observer in plane

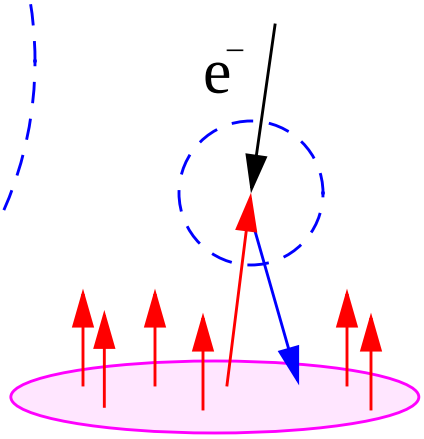

Galactic plane

Anisotropic/isotropic IC

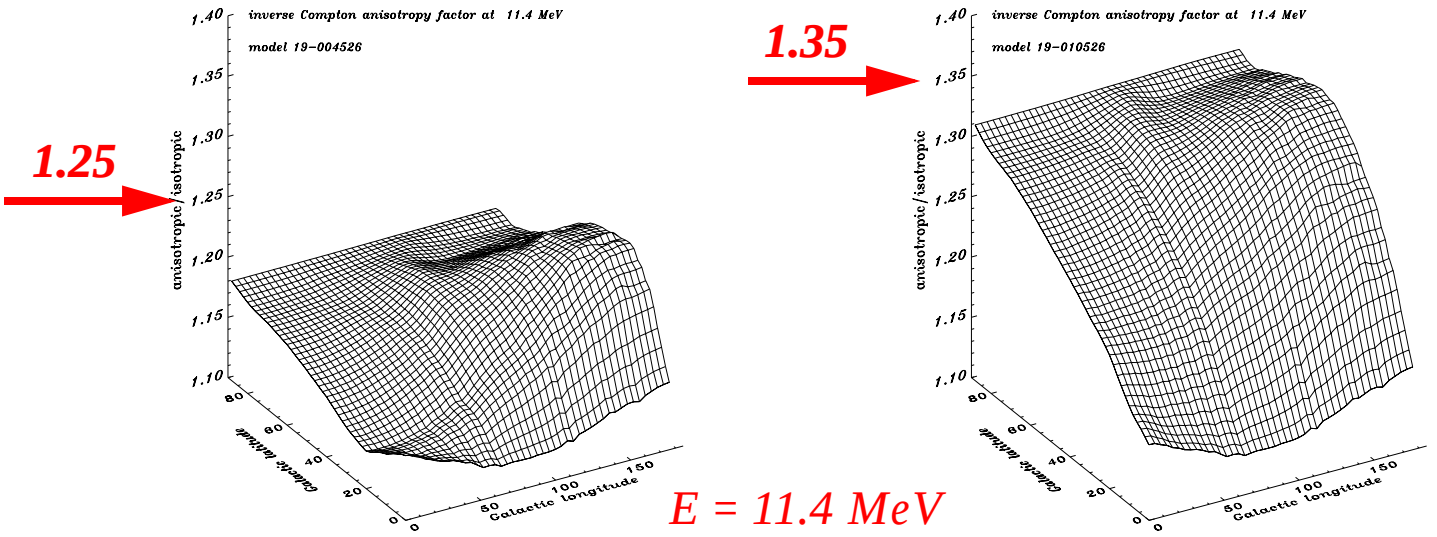

FIG. 5.— Latitude – longitude plot of the anisotropic/isotropic intensity ratio for 11.4 MeV γ-rays (ratio of the two sky maps). Halo size z_h = 4 kpc (left) and 10 kpc (right).

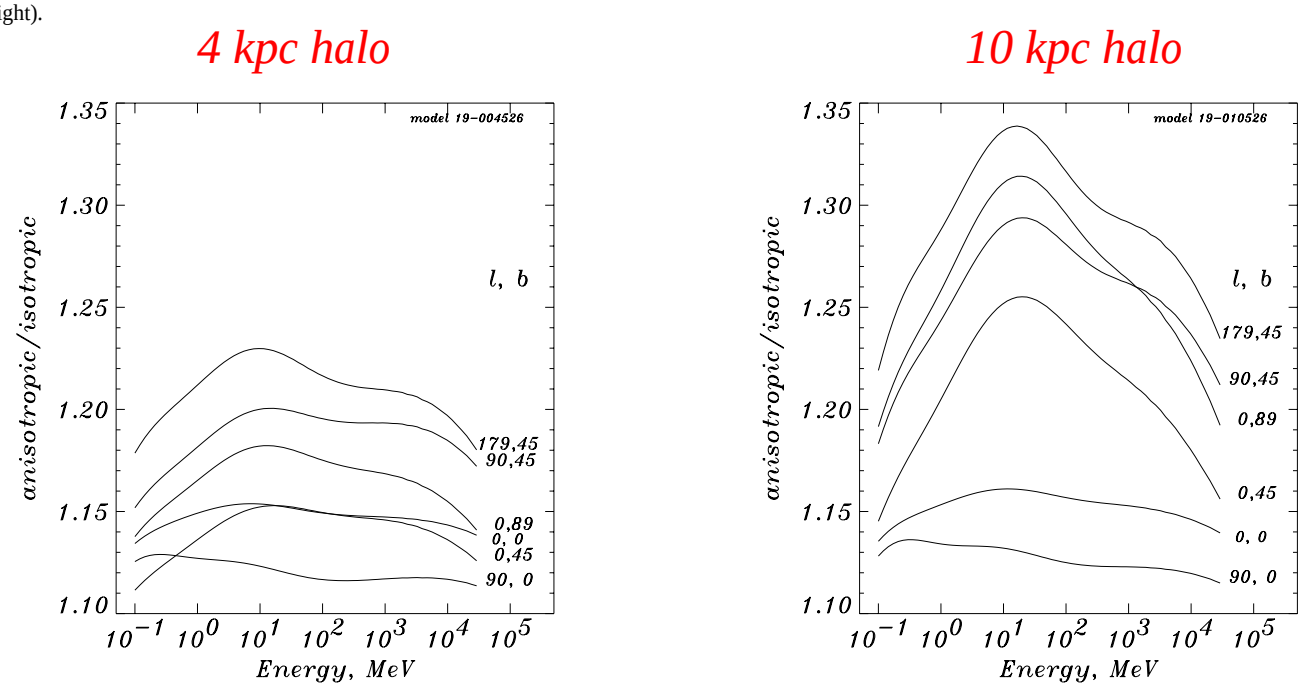

FIG. 6.— The intensity ratio vs. γ-ray energy for some direction as seen from the solar position. The corresponding Galactic coordinates (l, b) are shown near the right scale. Halo size z_h = 4 kpc (left) and 10 kpc (right).

Galactic CR distribution of Carbon-12 and Boron-10,11

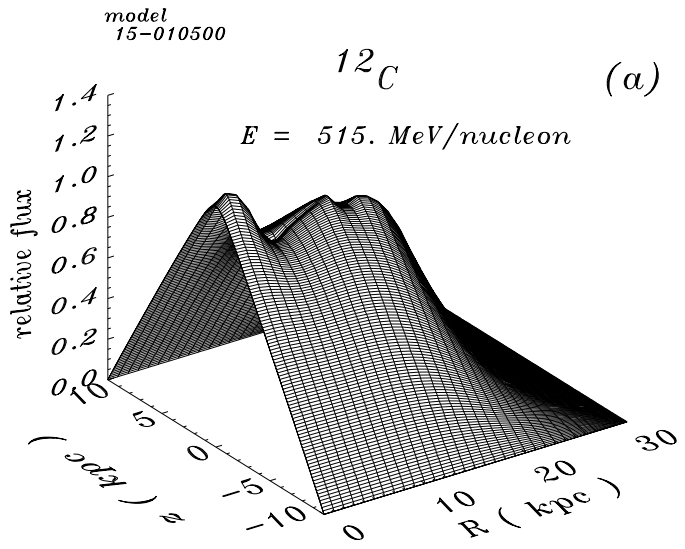

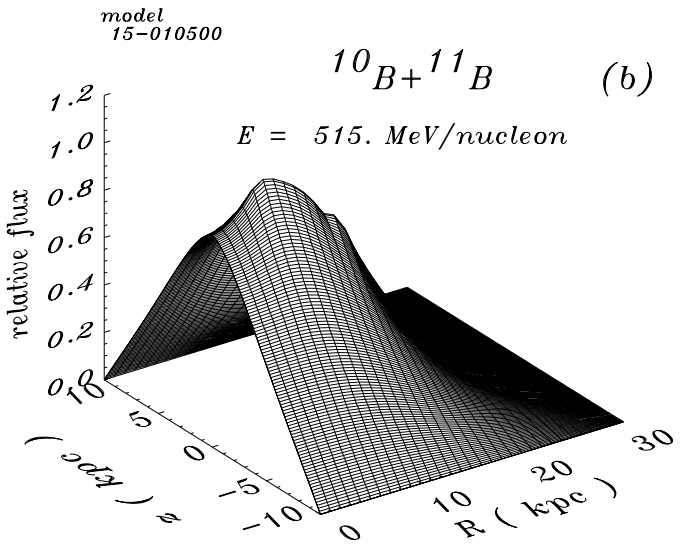

Table 1: The GALPROP parameters & constraints

Parameter	Constraints
Gas distribution (H2, HI, HII); He/H Galactic magnetic field model	Observations -”-
Interstellar radiation field (ISRF)	Observations + calculations
Particle injection spectra: Nucleons Electrons	 Local spectrum ? Diffuse gamma-ray emission Antiproton & positron measurements Local spectrum ? Synchrotron index measurements
Diffusion coefficient, Dxx **Reacceleration:** *Alfven velocity, Va* **Convection:** *break in the diffusion coeff.* *convection velocity @ z=0* *velocity gradient dV/dz*	Secondary/primary ratio (e.g. B/C) -”- -”- -”- -”-
Galactic halo radius, Rh Galactic halo height, Zh	= 30 kpc, fixed Radioactive isotopes (e.g. Be-10/Be-9)
Source distribution	deduced from EGRET >100 MeV data

Standard approach (e.g. 'leaky box')

$D_{xx} \propto v \quad ....R < R_0$

$D_{xx} \propto vR^{\mu} \quad ....R > R_0$

rigidity

$\mu = 0.6$

$R_0 = 4$ GeV/c

fitted from secondary/primary ratios

2 free parameters, ad hoc break

Diffusive reacceleration

$D_{xx} \; D_{pp} = p^2 V_A^2 / 9$

momentum diffusion coeff.

spatial diffusion coeff.

$D_{xx} \propto vR^{\mu}$

$\mu = 1/3$ (Kolmogorov)

1 free parameter, no break

physical basis

Conventional model

protons

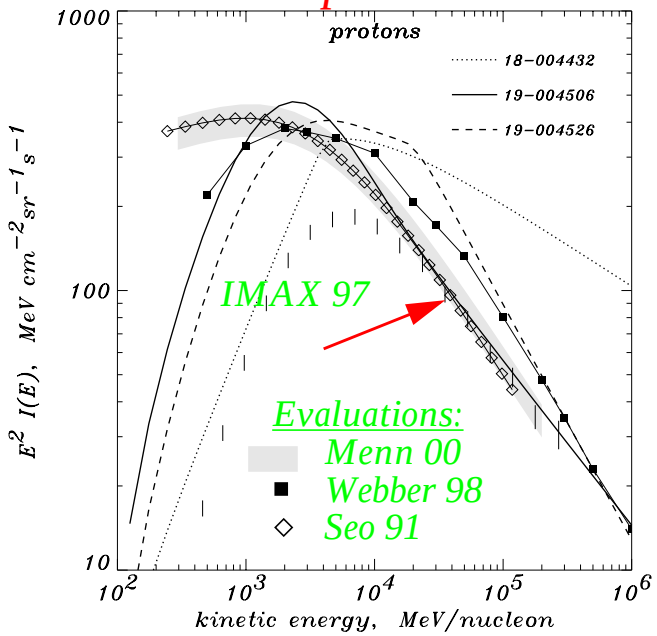

gammas

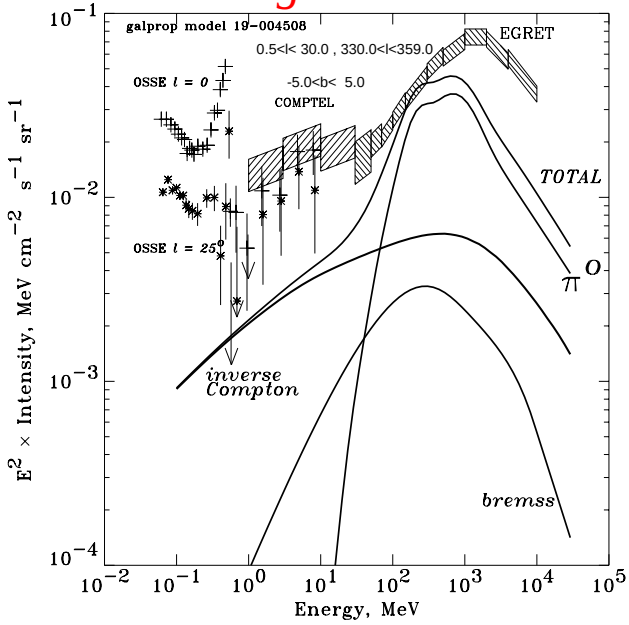

Tests of the nucleon spectrum

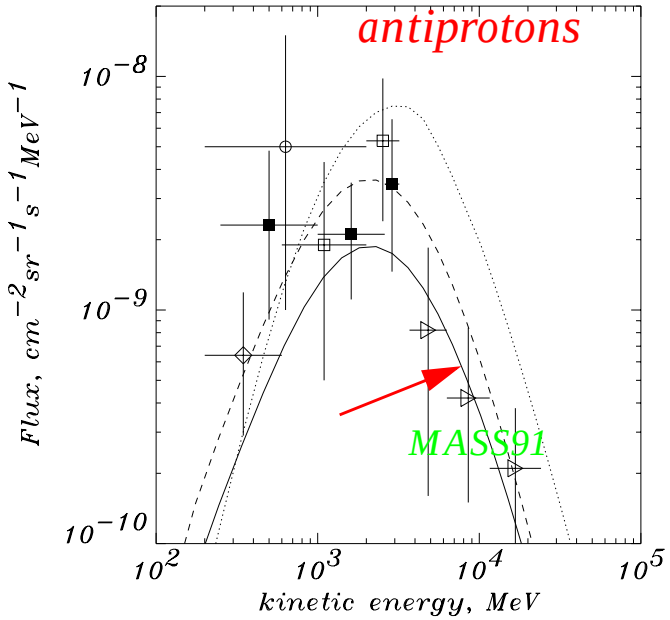

Interstellar positrons

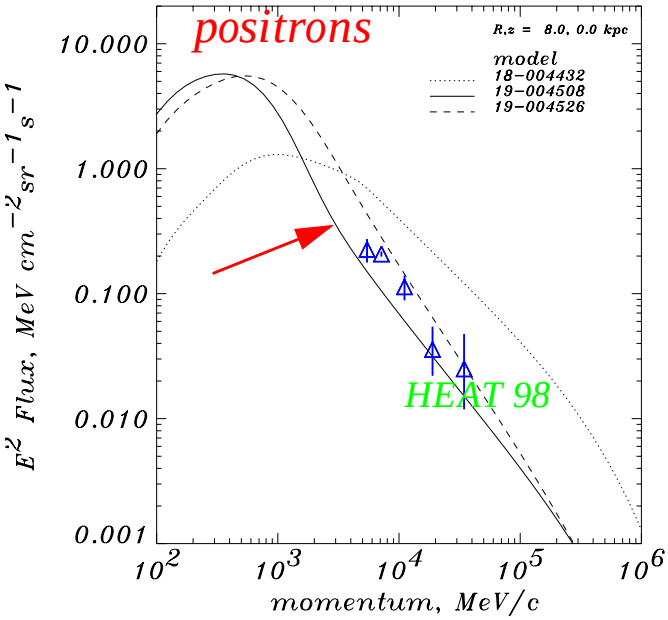

Hard X-rays -- soft gamma rays: unresolved point sources vs. diffuse emission

RXTE/OSSE (Kinzer et al. 1999; Valinia et al. 2000):

- Bright sources contribute 46% at 60 keV and 20% at 100 keV
- A variable component dominates at 10 keV-200 keV: exponentially cut off power law
- Hard component dominates above 500 keV

Yamasaki et al. 1997- diffuse hard X-rays:

- Unresolved point sources ~20%
- Young electrons in SNRs - the rest; -- still point sources !

Our result: changeover probably occurs at MeV energies

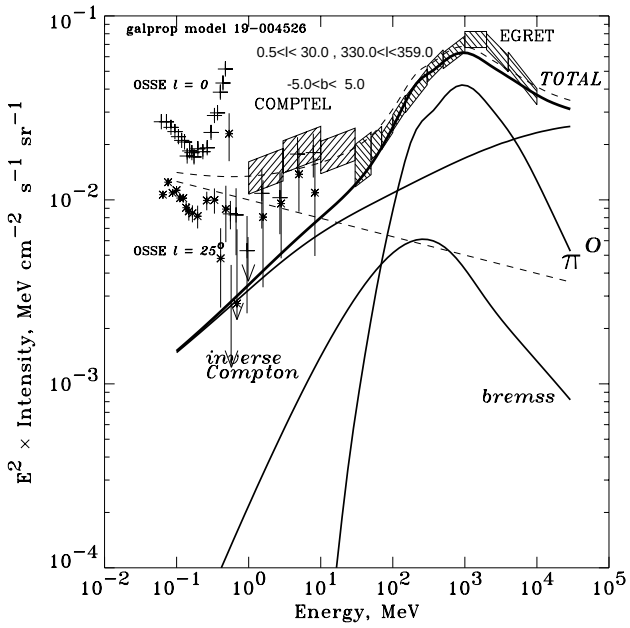

Diffuse emission + a few dosen of Crab-like sources

Hard Electrons model

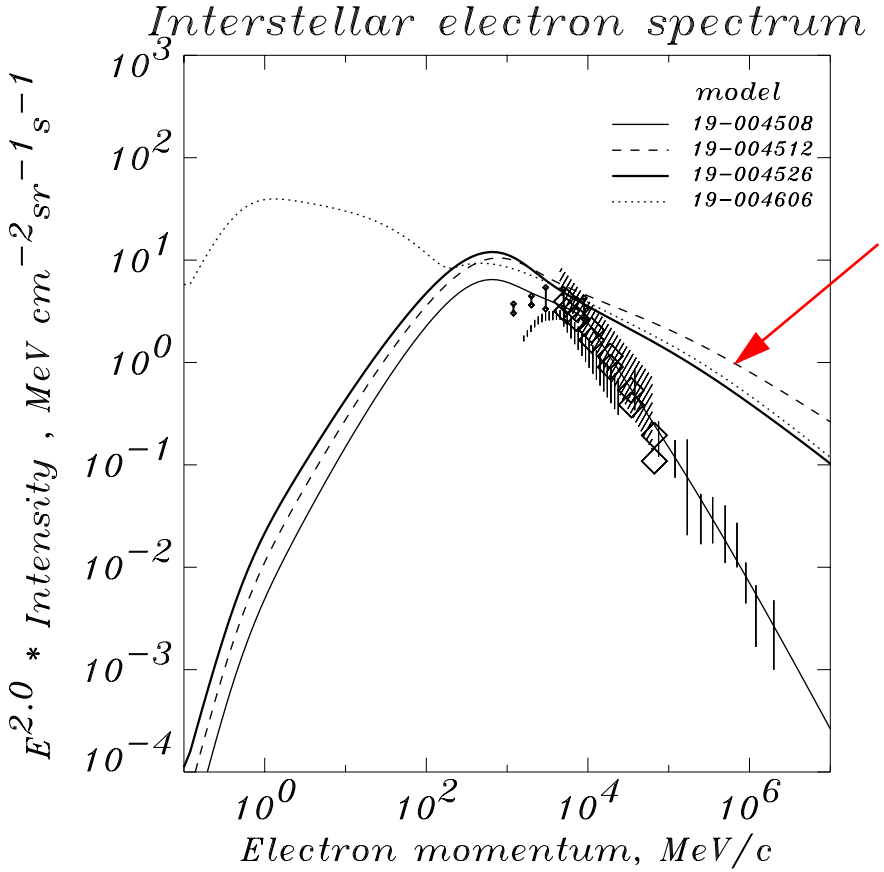

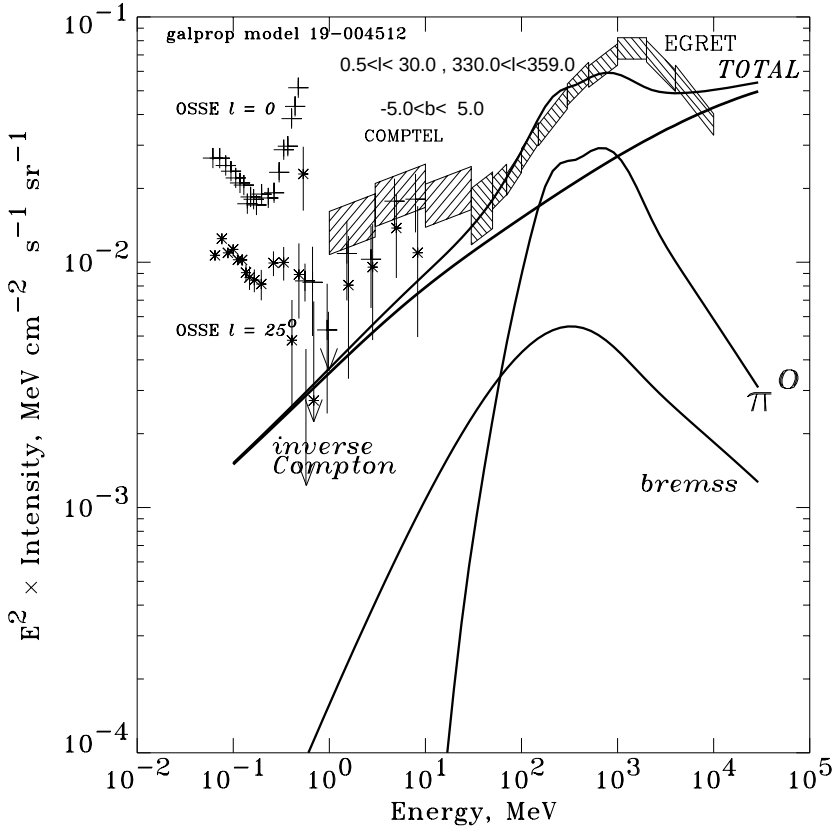

Hard Nucleons model

protons

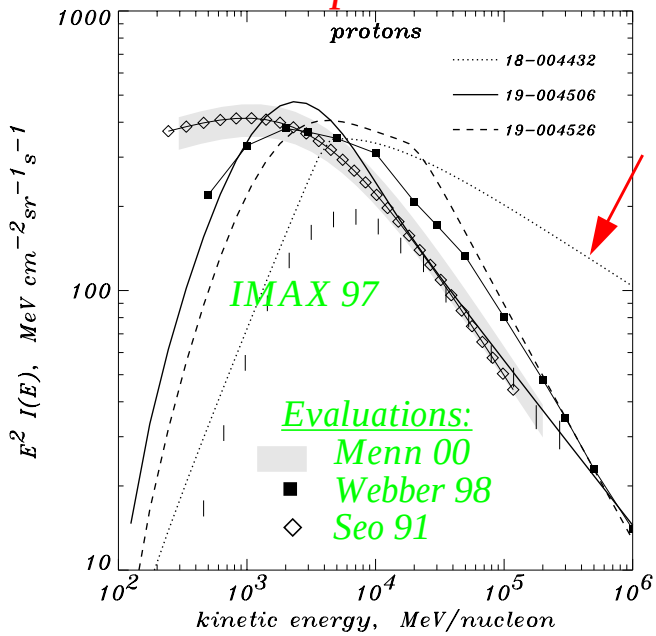

gammas

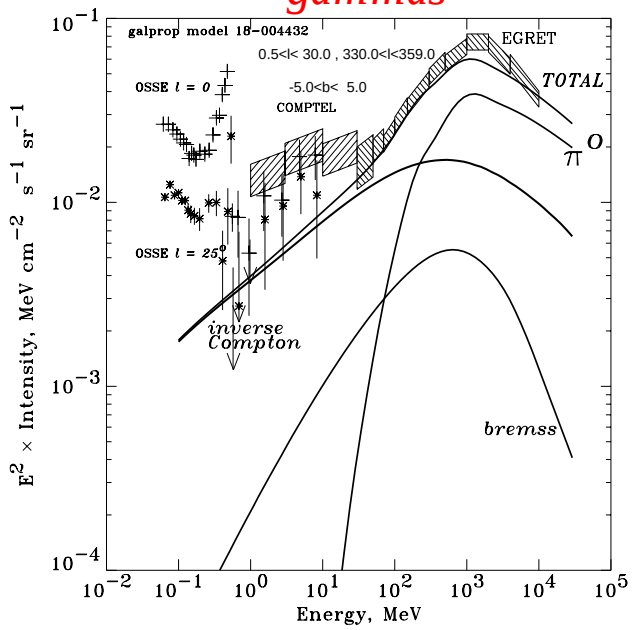

Tests of the nucleon spectrum

antiprotons

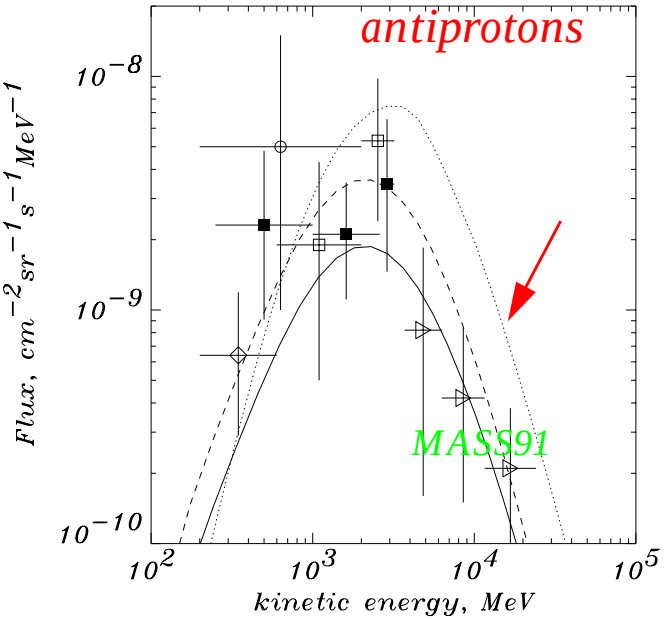

Interstellar positrons

positrons

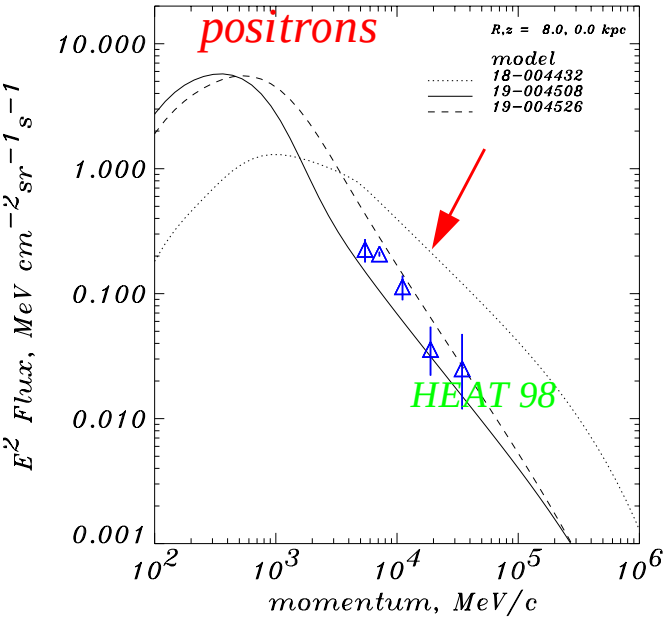

Interstellar electron spectra

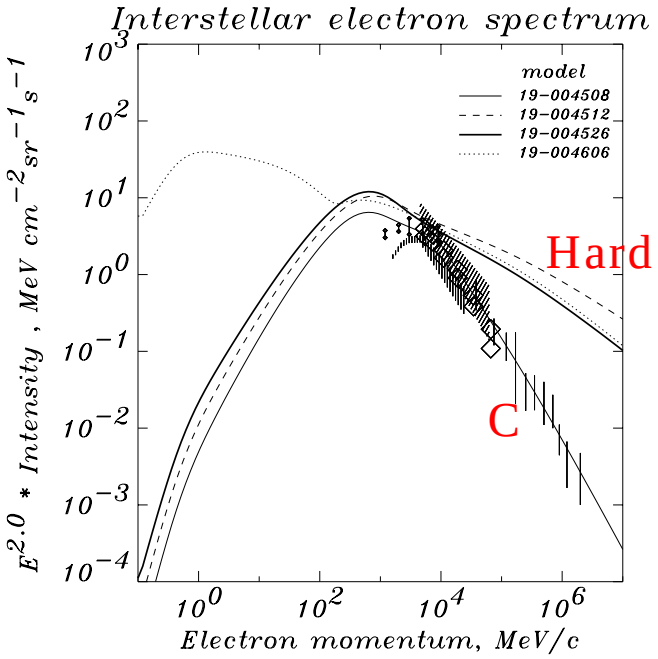

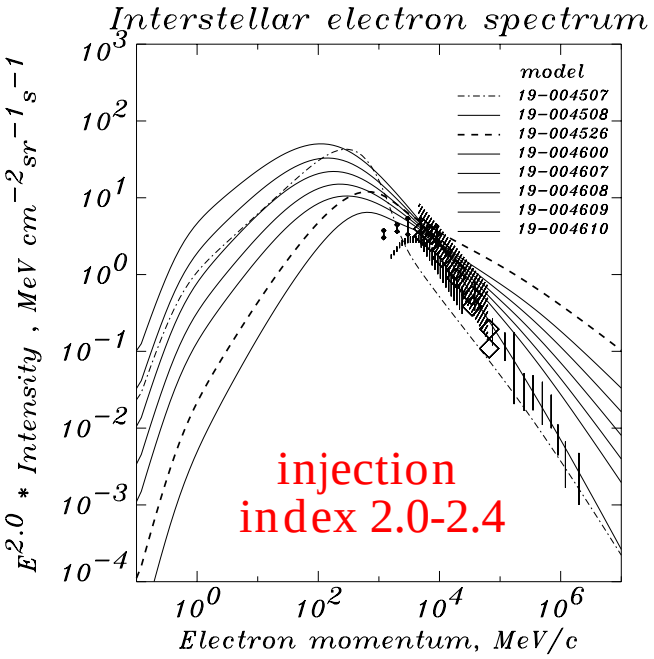

Synchrotron spectral index

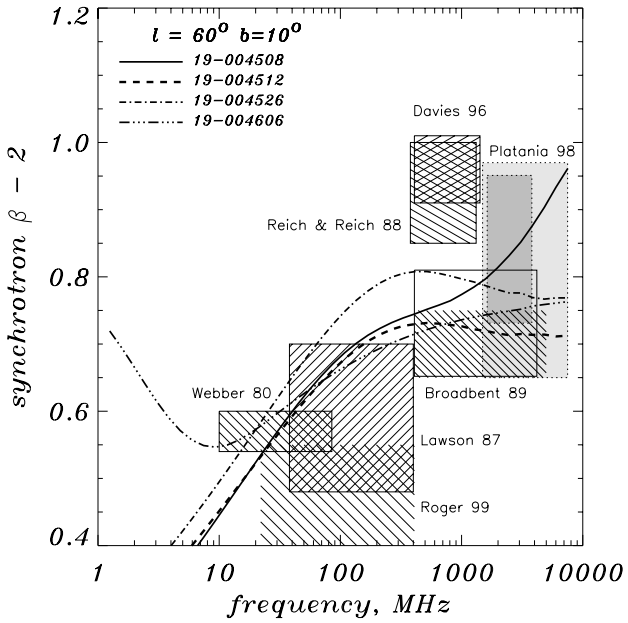

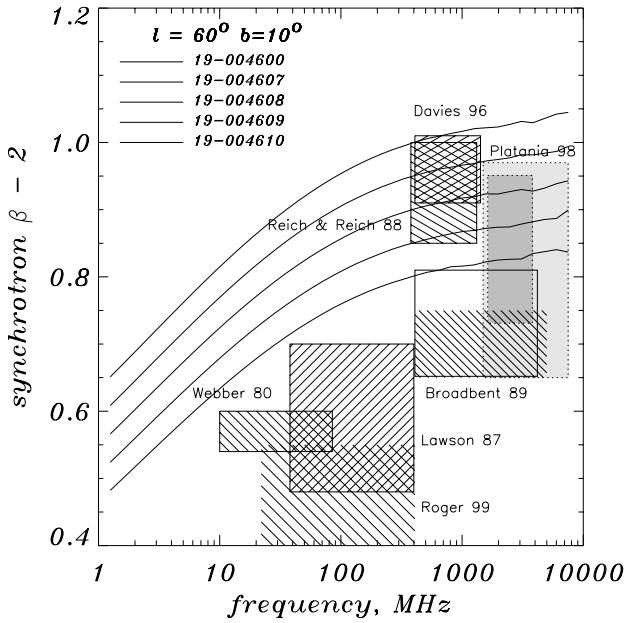

Hard Electrons & Modified Nucleons model

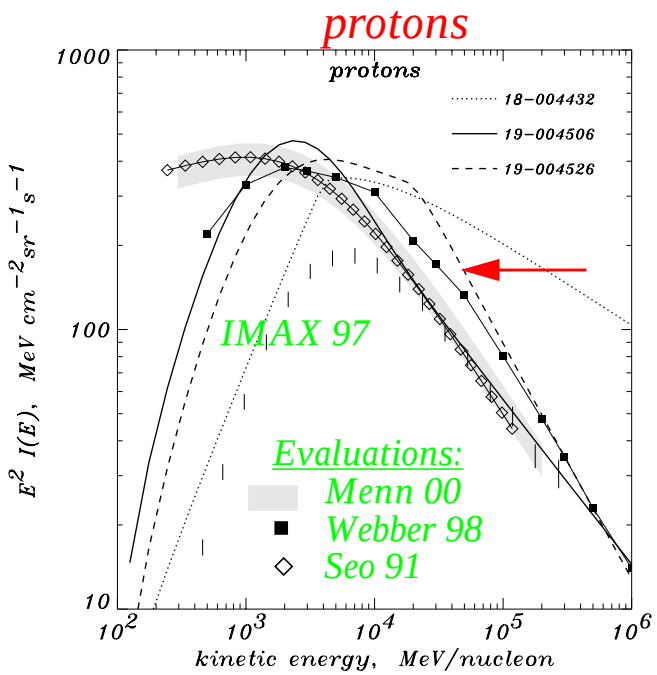

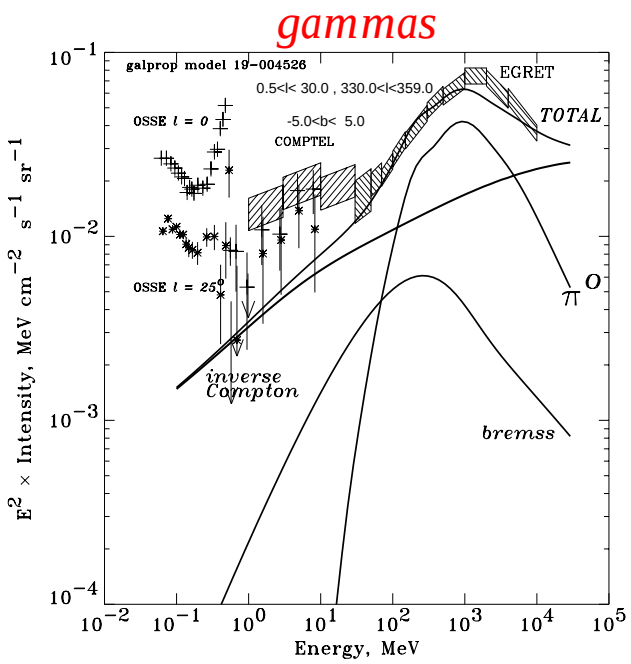

Tests of the nucleon spectrum

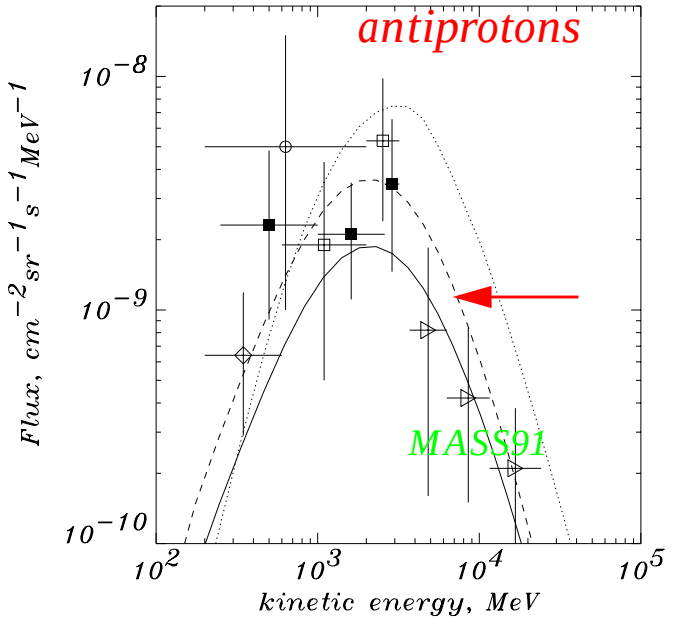

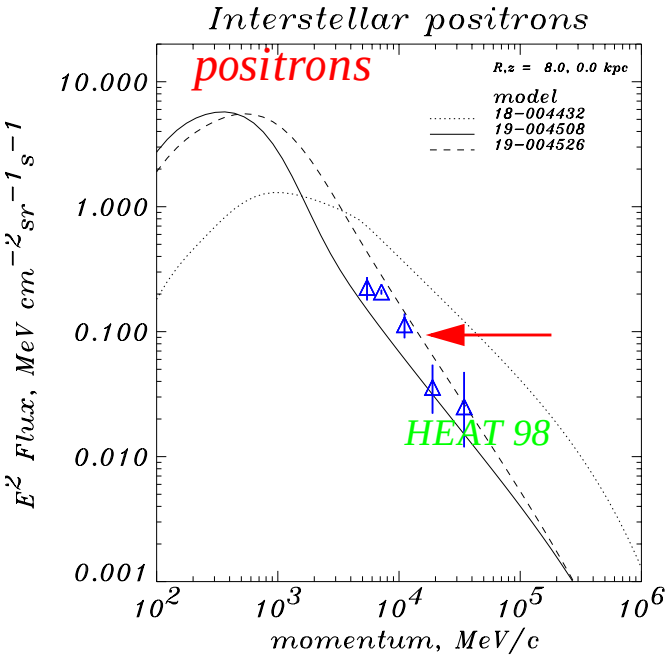

Magnetic field distribution

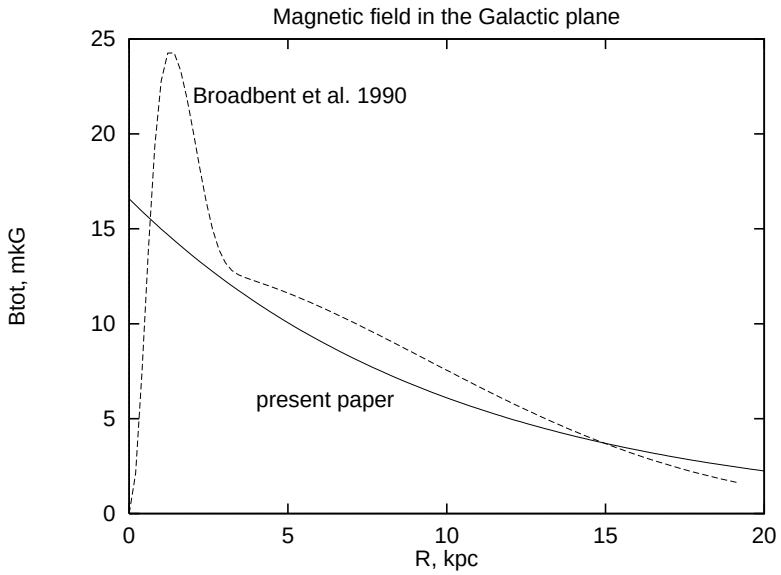

Intensity profiles of synchrotron emission @ 408 MHz

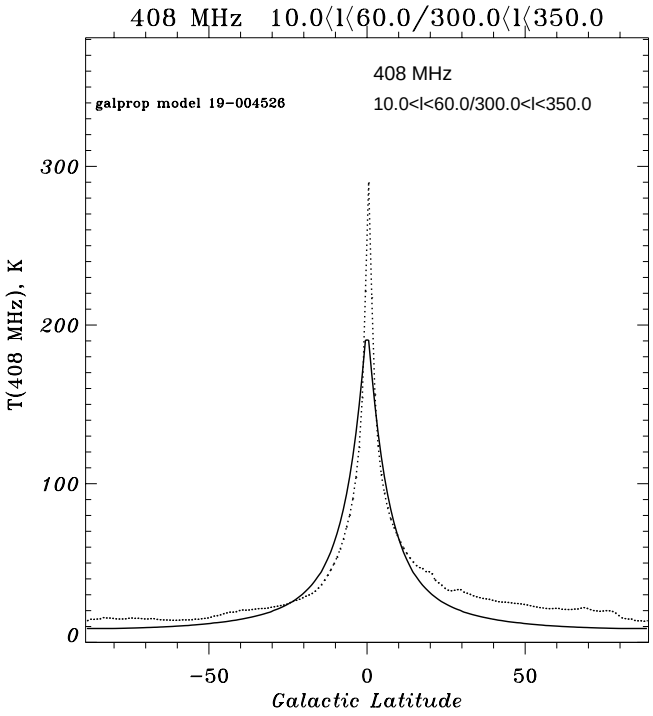

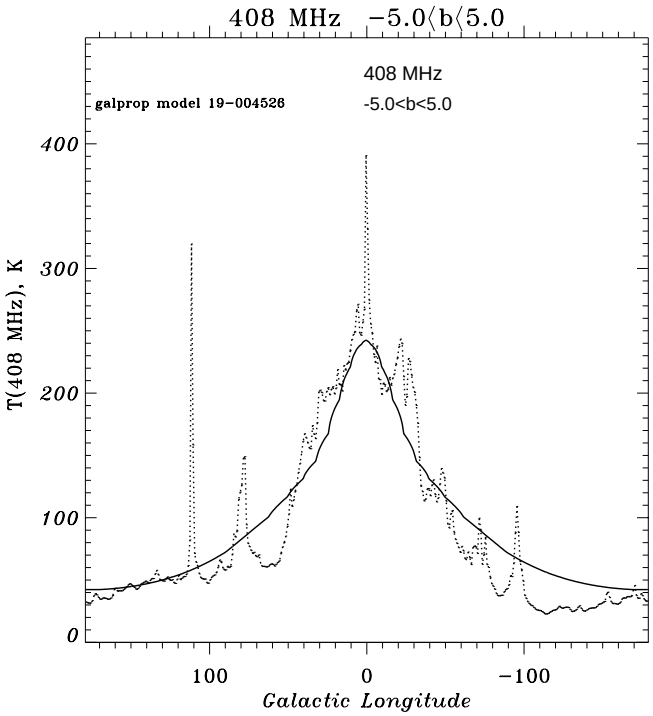

γ-ray profiles from EGRET Phase 1-4

compared to model with hard electron spectrum and modified nucleon spectrum

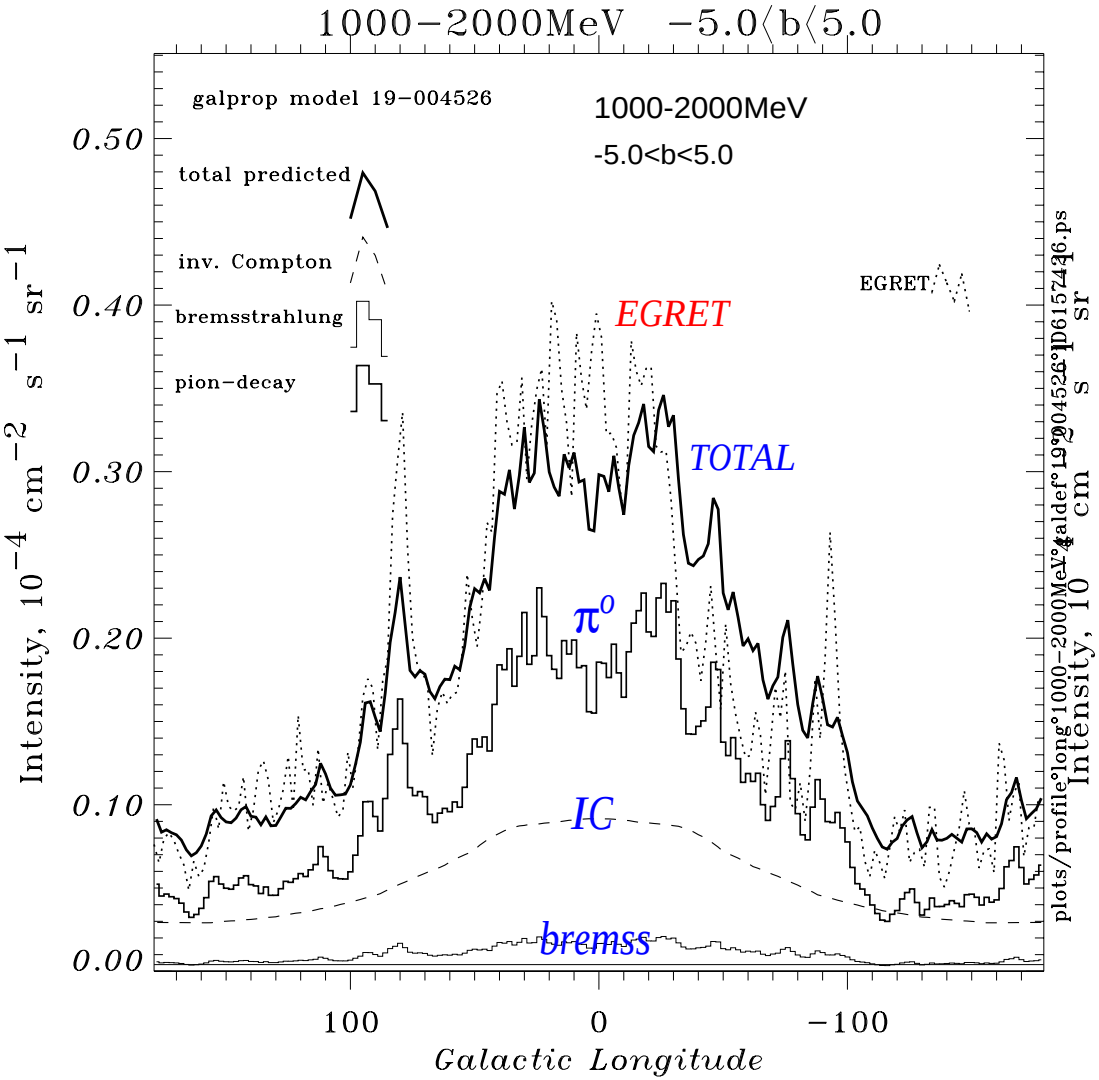

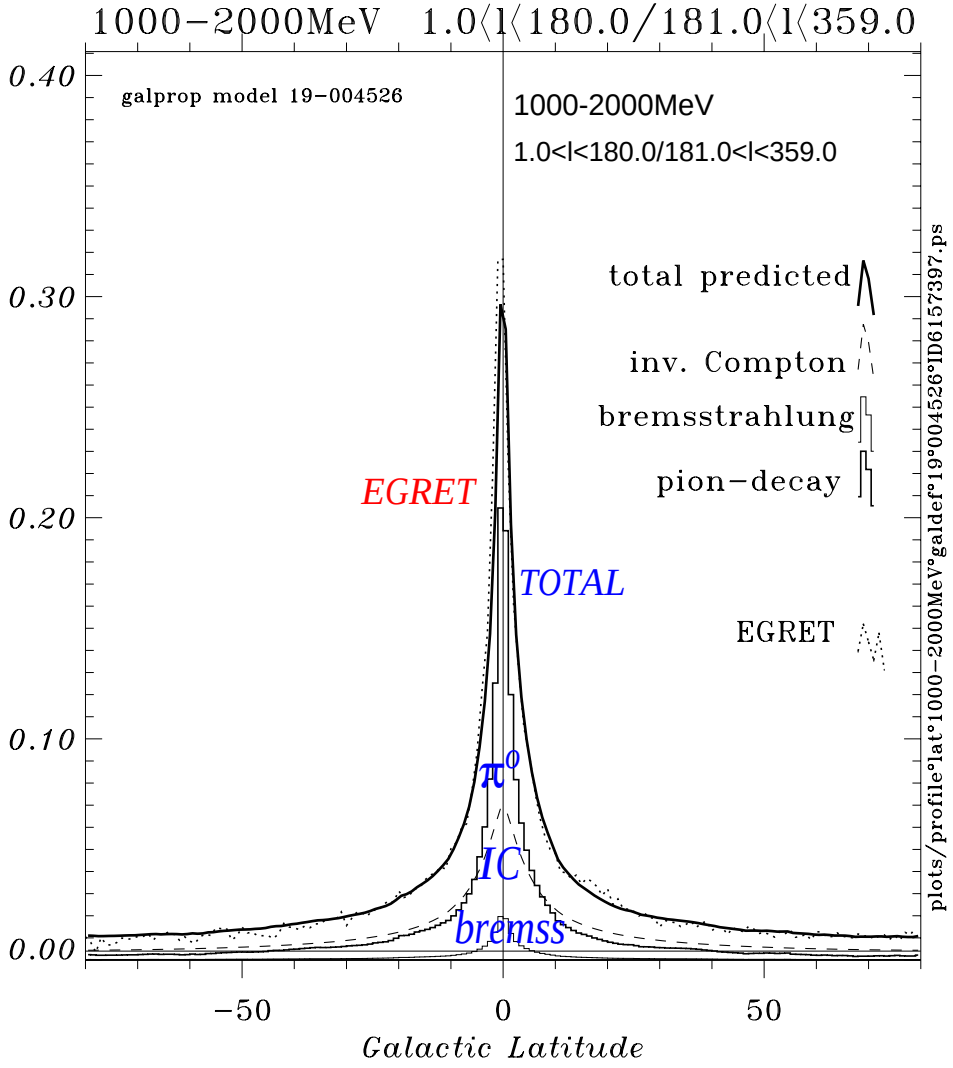

HIGH GALACTIC LATITUDE GAMMA RAYS

showing effect on inverse Compton scattering of anisotropic interstellar radiation field

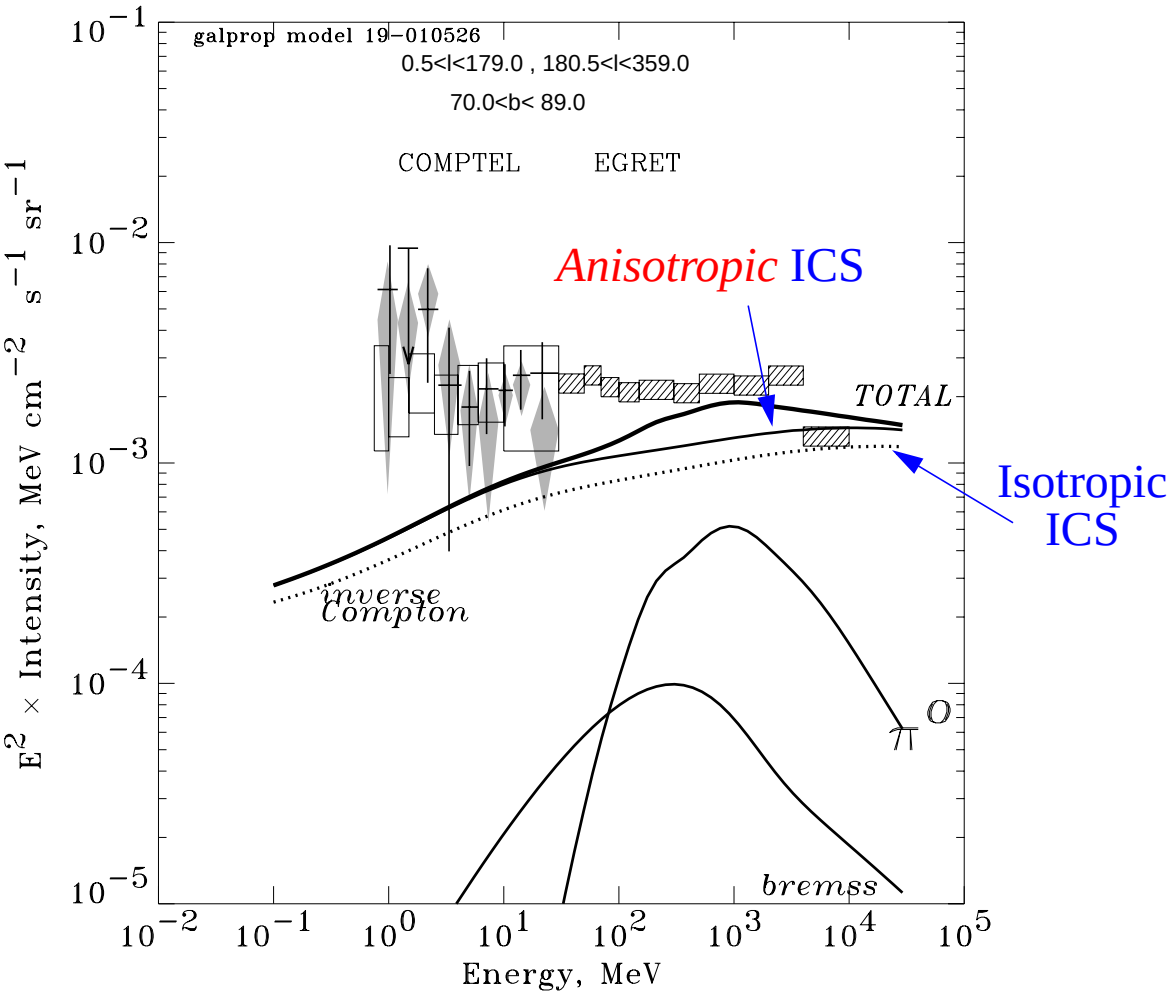

Electron spectra based on γ-rays

and

SNR acceleration from Baring et al. 1998

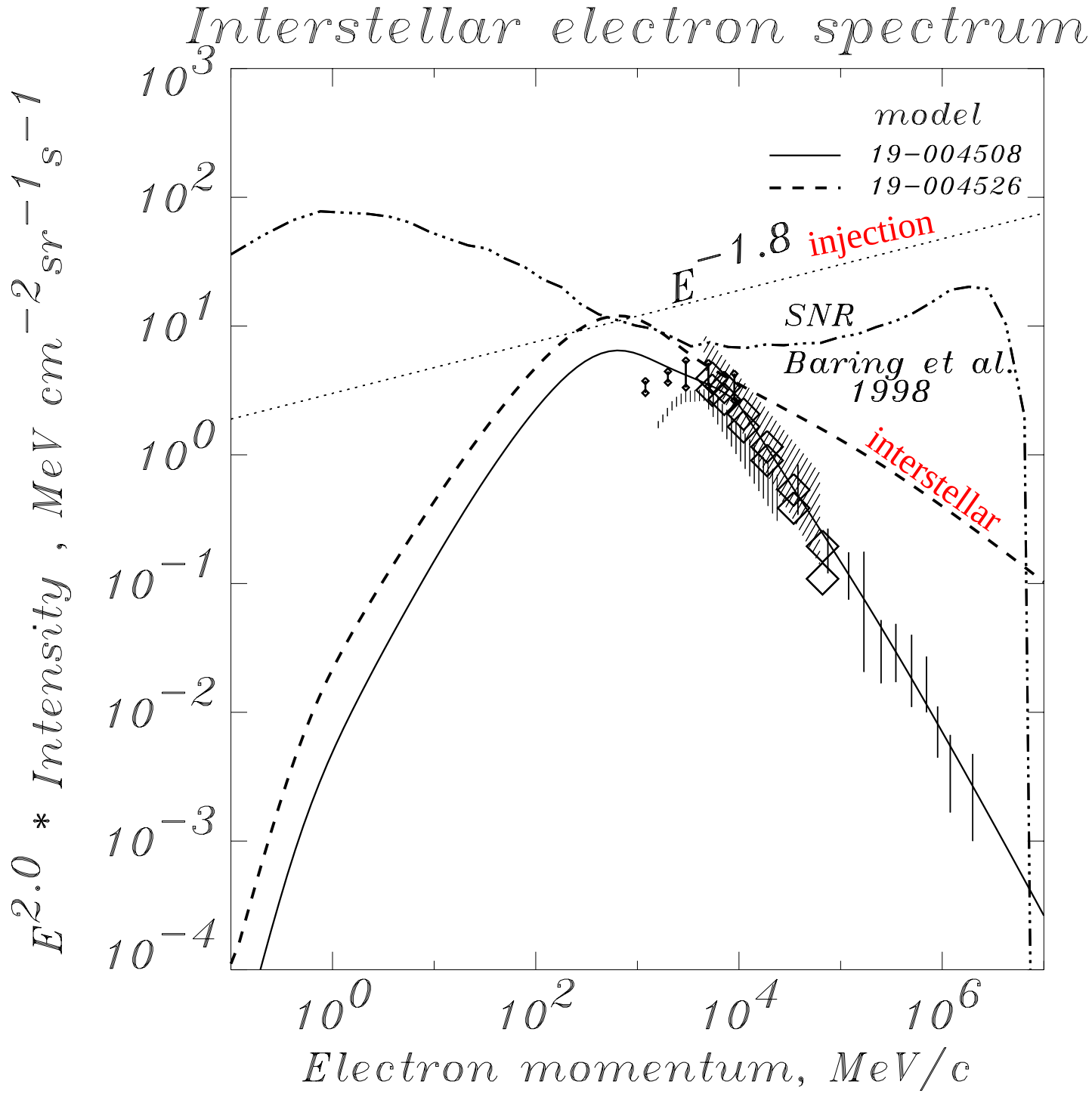

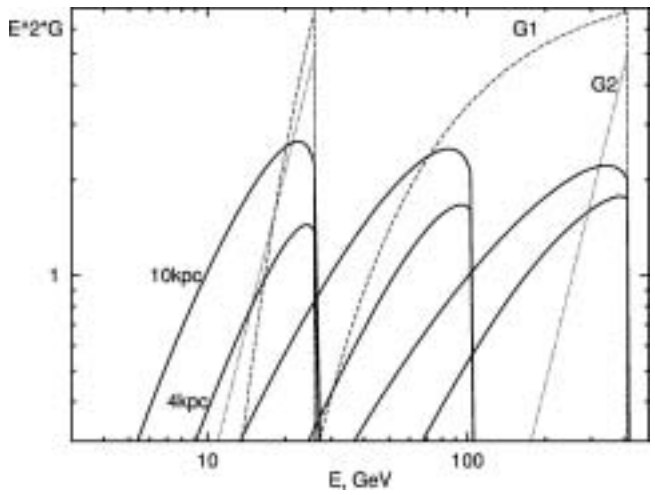

FIG. 2. Calculated G functions for the uniform dark matter distribution, $z_h=4$ kpc and 10 kpc, for $\epsilon=25.76$, 103.0, 412.1 GeV (solid lines). The leaky-box functions G_1 and G_2 are shown by dashed and dotted lines, respectively. The units of the abscissa are 10^{25} GeV cm sr^{-1}.

yr^{-1} GeV^{-1}, $\tau_0=10^7$ yr; G_2: $\xi = 1.52\times10^{-9}$ yr^{-1} GeV^{-1}, $\eta=2\times10^8$ yr GeV. It is clear that the leaky-box model does not work here, moreover a resonable fit to our G functions is impossible for any combination of ξ and τ_0 (or η). The difference in the normalization at maximum ($E=\epsilon$) is mainly connected with our accurate calculation of the ISRF which is responsible for the energy losses.

Figure 3 shows our calculated G functions for different models of the dark matter distribution: ''isothermal,''Evans, and alternative. The curves are shown for two halo sizes $z_h=4$ and 10 kpc and several energies $\epsilon=1.03$, 2.06, 5.15, 10.3, 25.8, 51.5, 103.0, 206.1, 412.1, 824.3 GeV. At high energies, increasing positron energy losses due to the IC scattering compete with the increasing diffusion coefficient, while at low energies increasing energy losses due to the Coulomb scattering and ionization [10] compete with energy gain due to reacceleration. The first effect leads to a smaller sensivity to the halo size at high energies. The second one becomes visible below ~5 GeV and is responsible for the appearance of accelerated particles with $E>\epsilon$.

It is interesting to note that for a given initial positron energy all three dark matter distributions provide very similar values for the maximum of the G function [on the $E^2G(E,\epsilon)$ scale], while their low-energy tails are different. This is a natural consequence of the large positron energy losses. Positrons contributing to the maximum of the G function originate in the solar neighborhood, where all models give the same dark matter mass density [see Eq. (4) for the definition of the G function]. The central mass density in these models is very different (Fig. 1), and therefore the shape of the tail is also different since it is produced by positrons originating in distant regions. As compared to the isothermal model, the Evans model produces sharper tails, while the alternative model gives more positrons in the low-energy tail. At intermediate energies (~10 GeV) where the energy losses are minimal, the difference between $z_h=4$ and

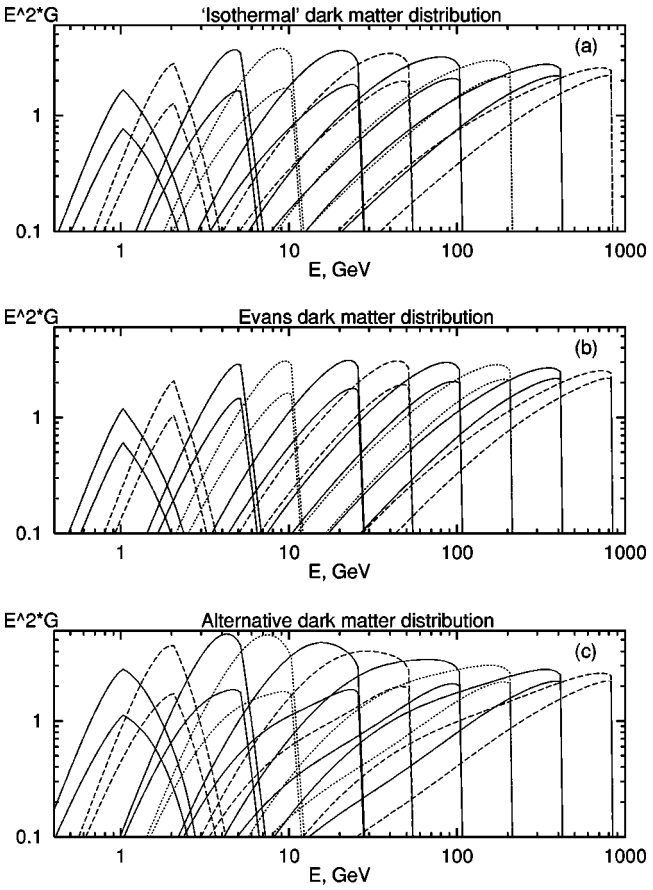

FIG. 3. Calculated G functions for different models of the dark matter distribution: (a) ''isothermal,'' (b) Evans, (c) alternative. Upper curves $z_h=10$ kpc, lower curves $z_h=4$ kpc, $\epsilon=1.03$, 2.06, 5.15, 10.3, 25.8, 51.5, 103.0, 206.1, 412.1, 824.3 GeV. The units of the abscissa are 10^{25} GeV cm sr^{-1}.

10 kpc is maximal. Also at these energies positrons from dark matter particle annihilations in the Galactic center can contribute to the predicted flux. This is clearly seen in the case of the alternative model with its very large central mass density [Fig. 3(c), $z_h=10$ kpc].

To provide the Green's function for an arbitrary positron energy, which is necessary for prediction of positron fluxes in the case of continuum positron source functions (as will be required if one considers secondary, tertiary, etc., decay products), we made a fit to our numerical results. Since a resonable fit using the leaky-box Green's functions is impossible we have chosen the function

$$G(E,\epsilon)=\frac{10^{25}}{E^2}\{10^{a\,\log^2E+b\,\log E+c}\theta(\epsilon-E) + 10^{w\,\log^2E+x\,\log E+y}\theta(E-\epsilon)\} \quad [\text{cm sr}^{-1}\ \text{GeV}^{-1}], \tag{10}$$

which allows us to fit our numerical functions with accuracy better than 10% over a decade in magnitude [on the $E^2G(E,\epsilon)$ scale]. Here the first term fits the low energy tail, the second term fits the right-hand-side part of the G func-

Positrons from neutralino annihilations in the Galactic halo

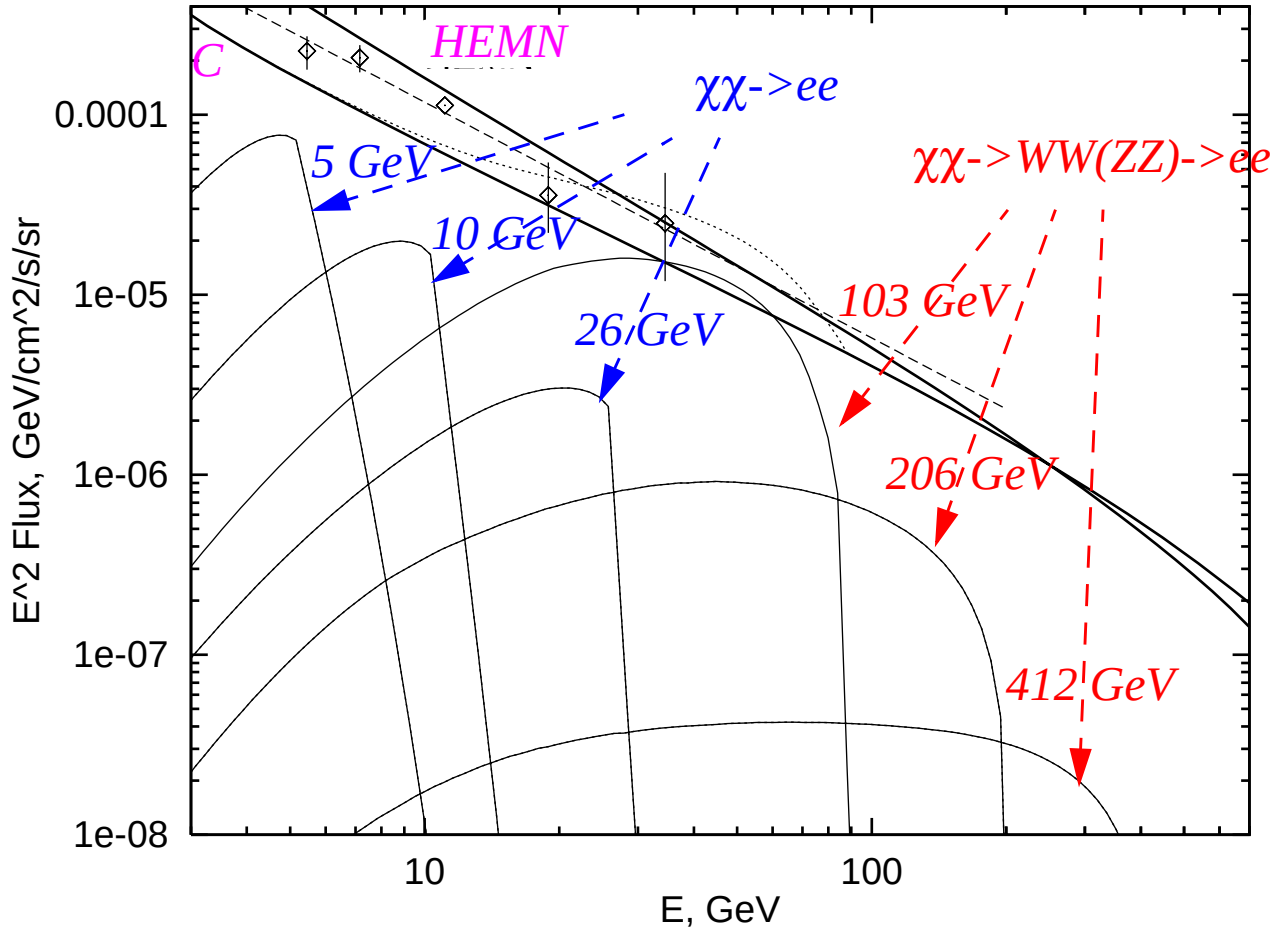

Positron signal & background estimates, data: HEAT'98.

* cross section: Kamionkowski & Turner 1991

- A significant detection of a signal requires favorable conditions and precise measurements
- *A correct interpretation* of measurements requires further developments in modelling production and propagation of CR species in the Galaxy

Interstellar radiation field

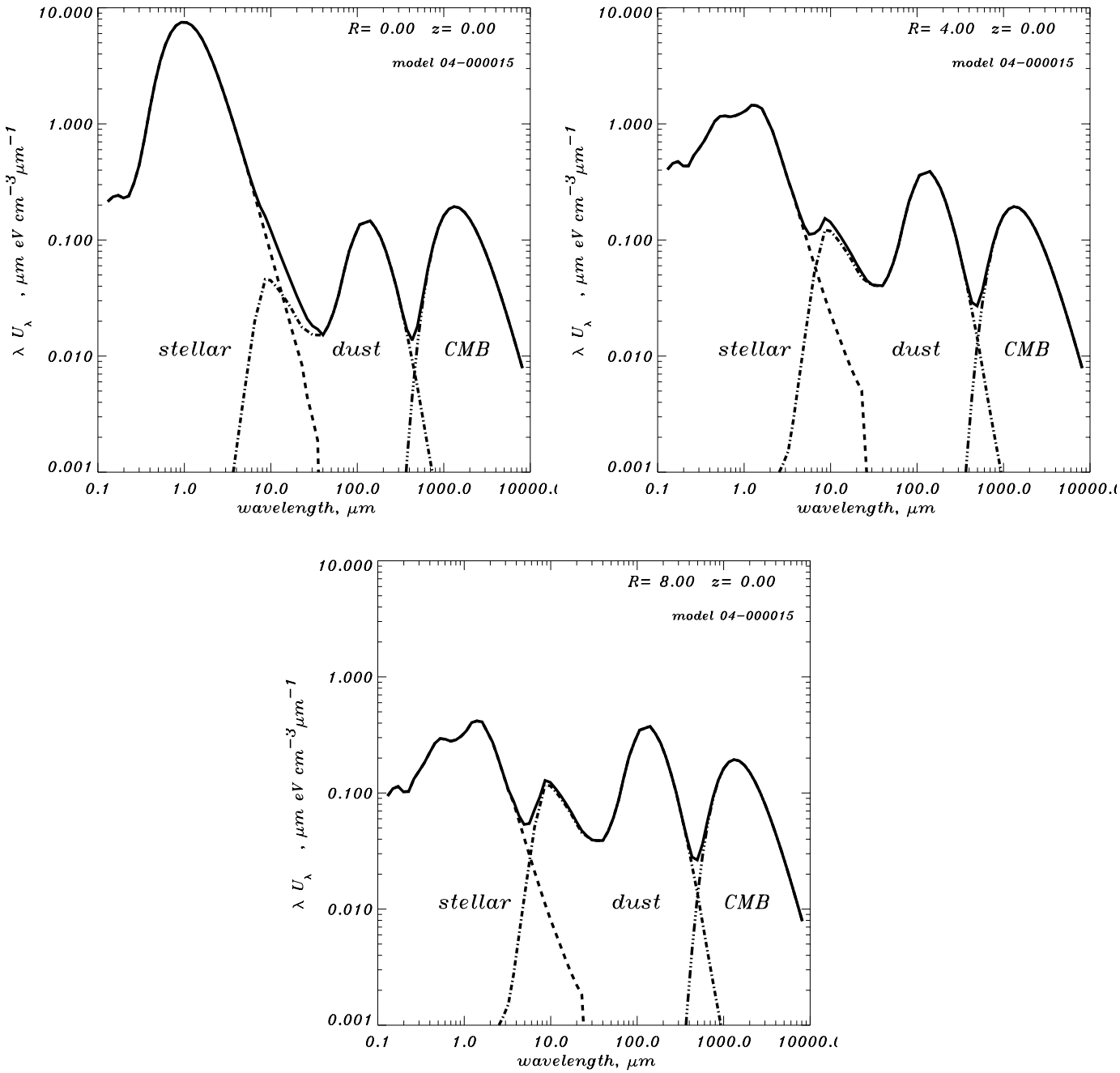

Figure 3: Differential energy density λu_λ (μm eV cm^{-3} μm^{-1}) of ISRF in the Galactic plane ($z = 0$) at $R = 0$ (top), 4 kpc (center), and 8 kpc (bottom). Shown are the contributions of stars (dashed), dust (dash-dot), CMB (dash-3-dots), and total (full line).

Standard approach (e.g. 'leaky box')

$D_{xx} \propto v \quad ....R < R_0$

$D_{xx} \propto vR^{\mu} \quad ....R > R_0$

rigidity

$\mu = 0.6$

$R_0 = 4$ GeV/c

fitted from secondary/primary ratios

2 free parameters, ad hoc break

Diffusive reacceleration

$D_{xx} \; D_{pp} = p^2 V_A^2 / 9$

momentum diffusion coeff.

spatial diffusion coeff.

$D_{xx} \propto vR^{\mu}$

$\mu = 1/3$ (Kolmogorov)

1 free parameter, no break

physical basis

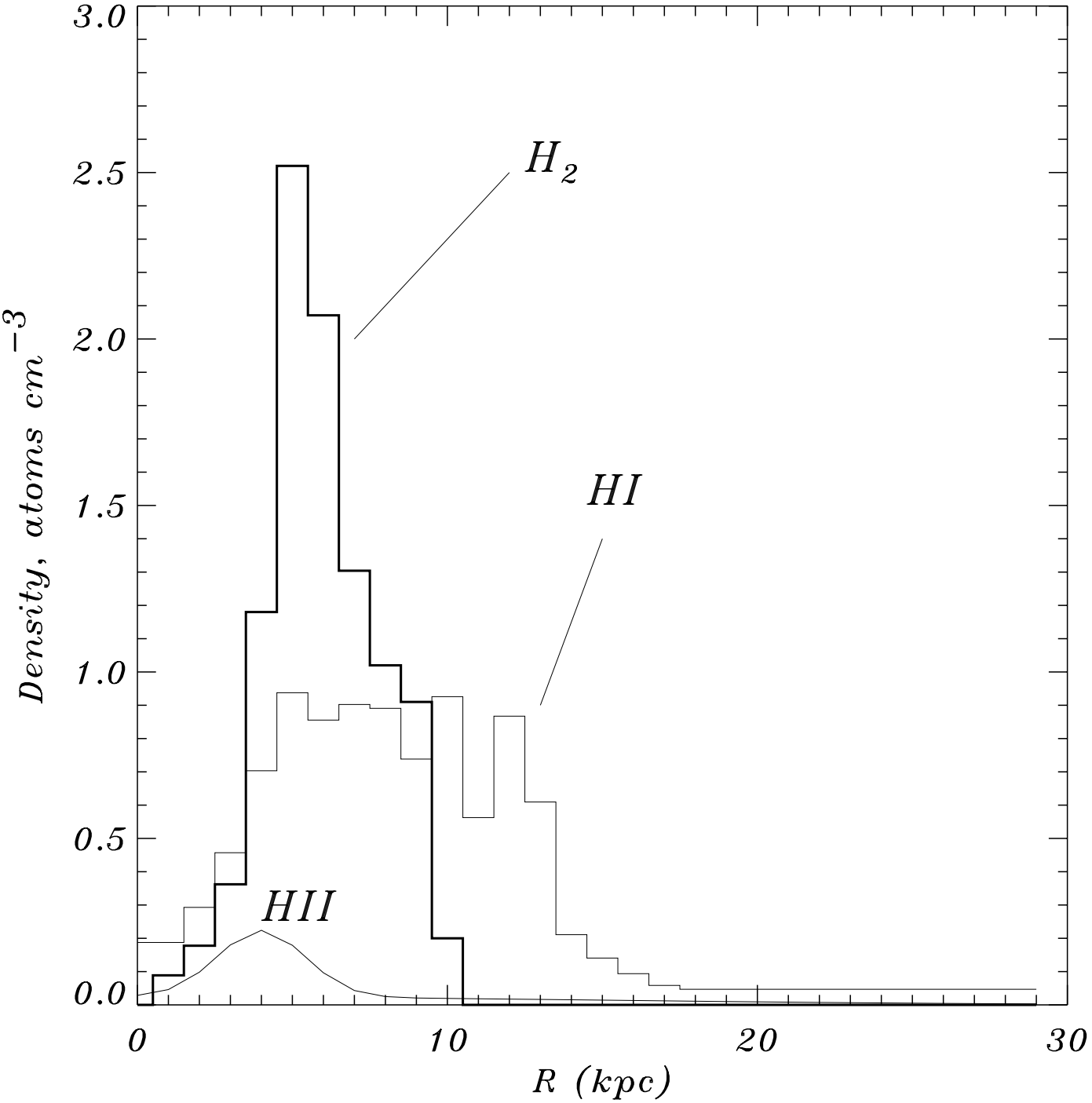
3.0
2.5
2.0
1.5
1.0
0.5
0.0
Density, atoms cm^{-3}
H_2
HI
HII
0
10
20
30
R (kpc)

SNRs are observed, and therefore observational incompleteness is still a problem for regions 1 and 3, where the completeness factors are lower. The scaled total number of shell SNRs in region 2 is $(56 \pm 4)/f_z$, where the error on the number of SNRs represents the uncertainty in the &-D relation and f_z represents the incompleteness due to the lack of selection e†ects compensation for the zero bins. For region 2, f_z B 0.96. If region 2 is considered representative of the entire Galaxy, then the total number of shell remnants for $r \leq 16$ kpc and & [5×10^{-23} W m^{-2} Hz^{-1} sr^{-1} is estimated to be $336/f_z$. The Monte Carlo simulation shows that this estimate is not very sensitive to the uncertainty in the &-D relation.

A weighted Ðt of the shell SNR surface density distribution in region 2, normalized to the surface density at the solar circle, was performed using the functional form employed by Stecker & Jones (1977):

$$f(r) = \left(\frac{r}{r_\odot}\right)^{\alpha} \exp\left(-\beta \frac{r - r_\odot}{r_\odot}\right), \qquad (14)$$

where $r_\odot = 8.5$ kpc is the SunÈGalactic center distance. We Ðnd that $\alpha = 2.00 \pm 0.67$ and $\beta = 3.53 \pm 0.77$; the radial scale length of the distribution is B7.0 kpc. The shape of the distribution is similar to that obtained by Kodiara (1974). The two distributions are shown in Figure 7a.

Equation (14) implies that the surface density is zero at $r = 0$. However, our data suggest that the surface density is not zero near the Galactic center. Therefore, we have used the following functional form to obtain a weighted Ðt to the unnormalized surface density distribution:

$$f(r) = A \sin\left(\frac{\pi r}{r_0} + h_0\right) e^{-\beta r}, \qquad (15)$$

where $A = 1.96 \pm 1.38$ kpc^{-2}, $r_0 = 17.2 \pm 1.9$ kpc, $h_0 = 0.08 \pm 0.33$, and $\beta = 0.13 \pm 0.08$ kpc^{-1}. This Ðt is valid for $r \leq r_0(1 - h_0/\pi)$, i.e., 16.8 kpc; $f(r) = 0$ beyond that. The data and Ðt are shown in Figure 7b.

The scale length of 7.0 kpc is consistent with that determined by previous studies. Green (1996b) used a simple model with SNRs distributed as a Gaussian in Galactic radius and compared the resulting longitudinal distribution with the observed SNR longitudinal distribution, obtaining a scale length of B7.0 kpc. However, no attempt was made to compensate for selection e†ects other than to use a &-limited sample. Li et al. (1991) used a more sophisticated model distributing SNRs in an exponential disk as well as in spiral arms. They incorporated a $1/d^2$ selection bias, assuming completeness out to $d = 3$ kpc. They then compared the longitudinal distribution given by the model with the observed SNR longitudinal distribution, obtaining a scale length of B5È9 kpc, depending on the model parameters. As Li et al. point out, the scale length of the Galactic stellar disk is $\sim$5 kpc, suggesting that the SNR scale length, as derived in this work and by Green (1996b) and Li et al. (1991), would indicate that the SNR distribution is not associated with the stellar disk population.

5. CONCLUSION

The catalog of known SNRs has continued to grow in size. The number of SNRs with reasonably determined distances has also increased. However, most distances given in the literature were calculated using older rotation curves. We have recalculated the distances, where necessary, using a modern rotation curve and used the updated distances to derive a new &-D relation for shell SNRs. This &-D relation, using a sample of 36 shell SNRs (37 including Cas A), yields a slope of [2.38 excluding Cas A and [2.64 with Cas A. When the 41 shell SNRs in the LMC and SMC are added to the sample, the slope is [2.41 with a smaller error. Using the &-D relation to estimate distances to individual remnants is viable only with the assumptions that all shell SNRs have the same radio luminosity dependence on linear diameter, have the same supernova explosion mechanism and energy, and are evolving into identical environments. We Ðnd that, on average, the error in the distance estimation to an individual SNR to be $\sim$40% when using our &-D relation. However, the error in deriving ensemble characteristics of SNRs such as the SNR surface density can be lower ($\sim$10%È20% for the mid-Galactic region). We attempt to compensate for observational selection e†ects inherent in SNR searches by employing a scaling method based on the sensitivity, angular resolution, and sky coverage of actual radio surveys. Using the updated distances, the new &-D relation, and the scale factors, the shell SNR surface density radial distribution was derived. The distribution peaks at $\sim$5 kpc and has a scale length of $\sim$7.0 kpc.

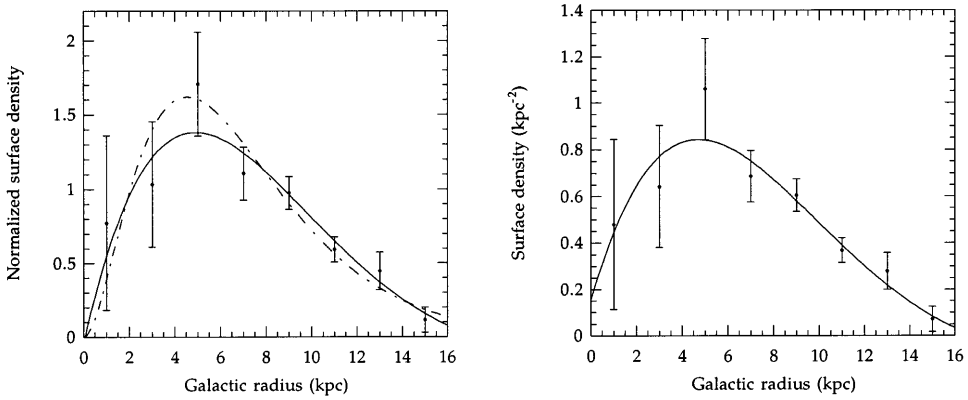

FIG. 7.È The SNR density radial distribution for region 2 using the new distances and compensation for selection e†ects. (a) The distribution derived in this work (solid line and data points) and that of Kodaira (1974) (dashed line), both normalized to the density at the radius of the solar circle. (b) The unnormalized data points and the Ðt to eq. (15).

$\overline{p}/p$ for various nucleon spectra options for diffuse γ-rays

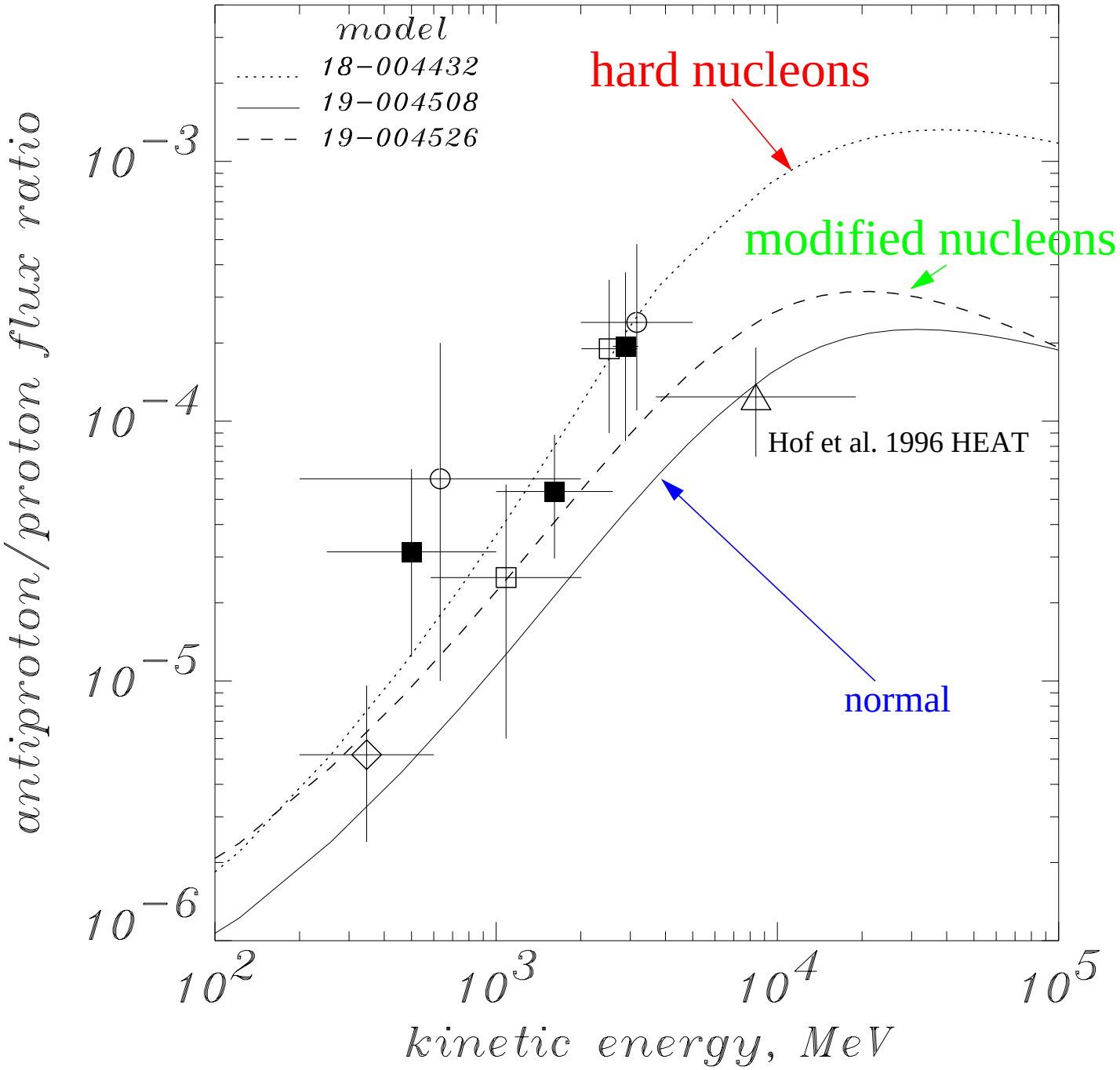

Latitude profile of γ-rays
for model with 4 kpc halo

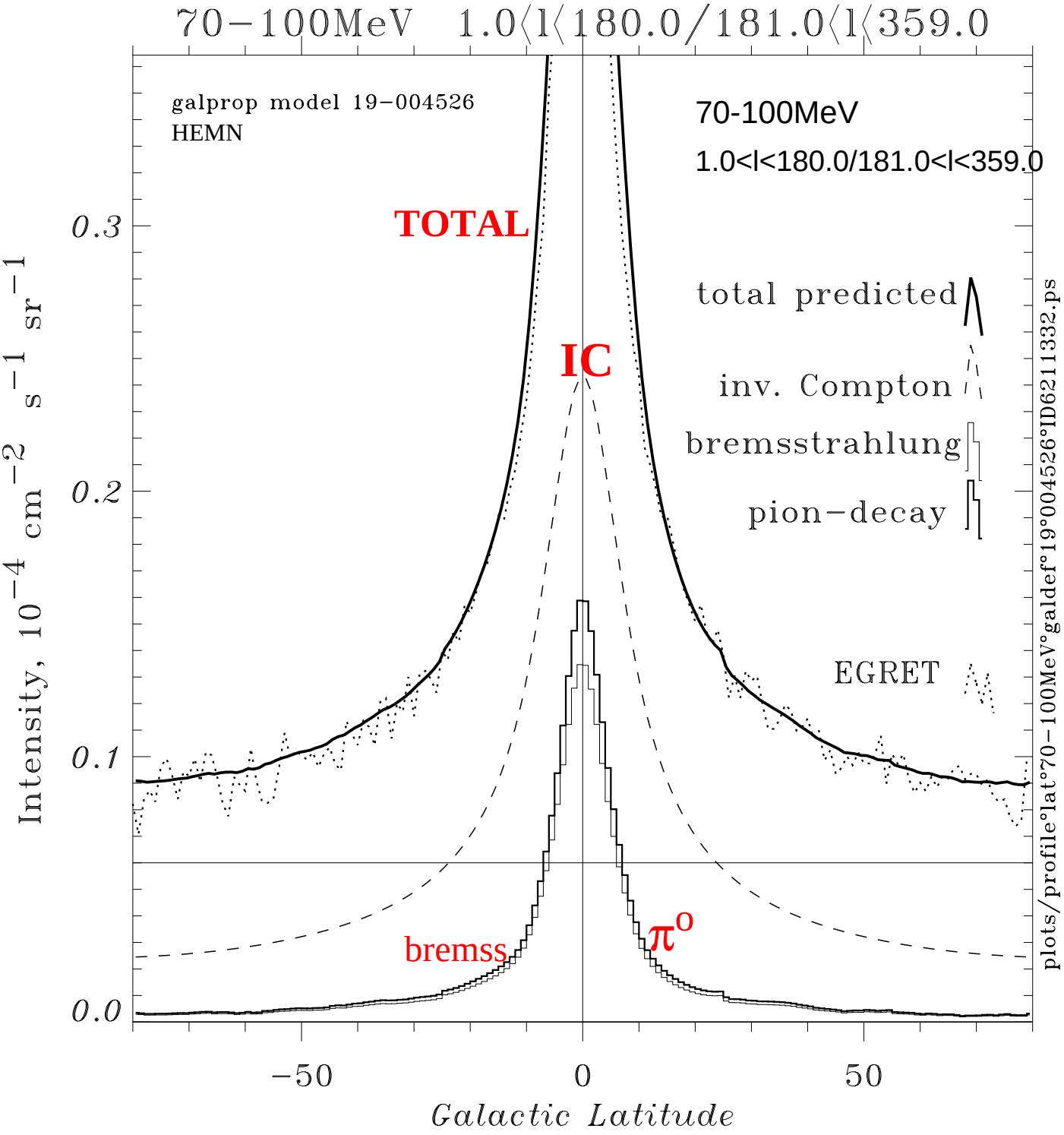

Table 1. Parameters and objectives of models.

Model[a]	GALPROP code	z_h kpc	D_0 $\mathrm{cm^2\ s^{-1}}$	Injection index			Motivation/Comments
				electrons	protons	He	
C	19-004508	4	6×10^{28}	1.6/2.6[b]	2.25	2.45	matches local electron, nucleon data and synchrotron; consistent with $\bar{p}$ and e^+ constraints
HN[f]	18-004432	4	3.5×10^{28}	2.0/2.4[b]	1.7	1.7	matches high-energy γ-rays using hard nucleon spectrum; inconsistent with $\bar{p}$ and e^+ constraints
HE[c]	19-004512	4	6×10^{28}	1.7	2.25	2.45	matches high-energy γ-rays using hard electron spectrum
HEMN	19-004526	4	6×10^{28}	1.8	1.8/2.5[d]	1.8/2.5[d]	optimized to match high-energy γ-rays using hard electron spectrum and broken nucleon spectrum; consistent with $\bar{p}$ and e^+ constraints
HELH	19-010526	10	12×10^{28}	1.8	1.8/2.5[d]	1.8/2.5[d]	HEMN with large halo
SE	19-004606	4	6×10^{28}	3.2/1.8[e]	2.25	2.45	matches low energy γ-rays using upturn in electron spectrum

[a]Propagation parameters are given in SM98 (C, HE, HEMN models: 15-004500; HELH: 15-010500; HN: 15-004100). All models except SE and HN are with reacceleration (Alfvén speed $v_A = 20$ km $\mathrm{s^{-1}}$). D_0 is the diffusion coefficient at 3 GV (5 GV for HN model). SE: $\delta = 1/3$, no reacceleration.

[b]Electron injection index shown is below/above 10 GeV.

[c]Nucleon spectrum normalization is 0.8 relative to model C.

[d]Injection index shown is below/above 20 GeV/nucleon.

[e]Electron injection index shown is below/above 200 MeV.

[f]$\delta = -0.60/0.60$ below/above 5 GV, no convection.